SPACE TELESCOPE SCIENCE INSTITUTE
Operated for NASA by AURA

Instrument Science Report WFC3 2005-25

WFC3-IR Thermal Vacuum Testing: IR Channel Dark Current

B. Hilbert and M. Robberto
September 9, 2005

ABSTRACT

During the 2004 thermal vacuum testing campaign, a series of tests were performed in order to analyze the dark current behavior of the WFC3's IR channel with the FPA64 detector. These tests included investigations of the dark current levels during each of the IR channel's readout sample sequences as well as dark current variations between nominal and non-nominal operating temperatures. For most sample sequences, the measured dark current at nominal operating temperature (150 K) was ~0.10-0.21 e^-/sec/pix. This value is a factor of 3-5 larger than the FPA-only dark current of ~0.04 e^-/sec/pix measured at the Detector Characterization Laboratory (DCL) earlier in the year, (DCL, 2003) but includes the thermal contribution from the cold enclosure. The total dark current signal therefore, meets the CEI Specification of 0.4 e^-/sec/pix, and the goal of 0.20 e^-/sec/pix. The data also revealed some unexpected effects, including a cyclical variation of dark current correlated with cold enclosure temperature and TEC voltage, as well as bad pixel masks that change with time.

1. Introduction

WFC3's first thermal vacuum testing campaign took place during September and October, 2004. This was the first opportunity to characterize the fully integrated IR channel. Eleven distinct tests were performed, each of which was contained within its own Science Mission Specification (SMS), to assess the dark current behavior.

2. Data

The dark current test data included ramps taken using every sample sequence available to general users. These are: RAPID, SPARS10, SPARS25, SPARS50, SPARS100, and SPARS200, in which the measured signal is sampled at regular intervals, with higher numbers meaning a longer time between samplings, and STEP25, STEP50, STEP100, STEP200, STEP400, MIF600, MIF900, MIF1200, and MIF1500, in which the detector signal is sampled at non-uniform intervals. The details of the sampling patterns are outlined in the OP-01 document (Baggett, W. 2003).

Besides exploring the dark current behavior associated with each sample sequence at nominal temperature and full-frame mode, data were taken at non-nominal temperatures, and in subarray mode. A summary of the dark current data, grouped by SMS, is given in Table 1. All data were taken at the nominal gain of 2.5 e^-/ADU.

List of Observations

SMS	Filename Prefix	Sample Sequence	# Ramps	Temperature (^{o}C)	Subarray Size
IR01S02	ii0102	RAPID	1	-123^{o}C (nominal) and -127^{o}C	NA
		STEP400	1		NA
IR01S03	ii0103	RAPID	3	nominal	NA
		SPARS10	3	nominal	NA
		SPARS25	3	nominal	NA
		SPARS50	3	nominal	NA
		SPARS100	3	nominal	NA
		SPARS200	3	nominal	NA
IR01S04	ii0104	STEP25	3	nominal	NA
		STEP50	3	nominal	NA
		STEP100	3	nominal	NA
		STEP200	3	nominal	NA
		STEP400	3	nominal	NA
IR01S05	ii0105	MIF600	3	nominal	NA
		MIF900	3	nominal	NA
		MIF1200	3	nominal	NA
		MIF1500	3	nominal	NA

SMS	Filename Prefix	Sample Sequence	# Ramps	Temperature (^{o}C)	Subarray Size
IR01S06	ii0106	SPARS100	10	-123^{o}C to -126^{o}C	NA
IR01S07	ii0107	RAPID	30	nominal	64 x 64, 256 x 256 512 x 512
		RAPID	5	nominal	NA
		SPARS10	10	nominal	512 x 512
		SPARS10	5	nominal	NA
		STEP50	5	nominal	NA
IR01S08	ii0108	SPARS100	35	nominal	NA
IR01S09	ii0109	SPARS50	18	-120^{o}C to -121^{o}C	NA
Manual Darks	iird60	RAPID	10	nominal	NA
		STEP25	10	nominal	NA
		STEP100	10	nominal	NA
		STEP400	10	nominal	NA
		SPARS10	10	nominal	NA
		SPARS10	10	nominal	512 x 512
IR05S01	ii05	RAPID	34	nominal	64 x 64, 128 x 128, 256 x 256, 512 x 512
		STEP25	24	nominal	64 x 64, 128 x 128, 256 x 256, 512 x 512
IR04S01	ii04	RAPID	2	nominal	NA

Table 1. Contents of the SMSs used to collect the dark current data during the thermal vacuum testing.

3. Analysis

All data were reduced using the standard IR pipeline written in IDL (B. Hilbert, 2004). The reference pixel values were subtracted from the science pixels and the zeroth read was subtracted from each subsequent read, in order to provide bias and KTC noise correction. Cosmic ray effects were removed by analyzing the signal of each pixel up the ramp, and hot/dead pixels were flagged using a mask created from an earlier dark current test. For a

detailed description of the mask generation method, see section 3.2.1 below. Typically, masks created from IR01 data flagged ~8.3% (~85,000) of the total pixels as bad, with most (> 92%) of the bad pixels classified as hot pixels.

Finally, a line was fit to the signal measured in each pixel up the ramp and the dark current for the pixel was then calculated from the slope of the best-fit line. In this way, a dark current map of FPA64 was constructed for each ramp. An example dark map, calculated from a SPARS200 ramp, is shown in Figure 1.

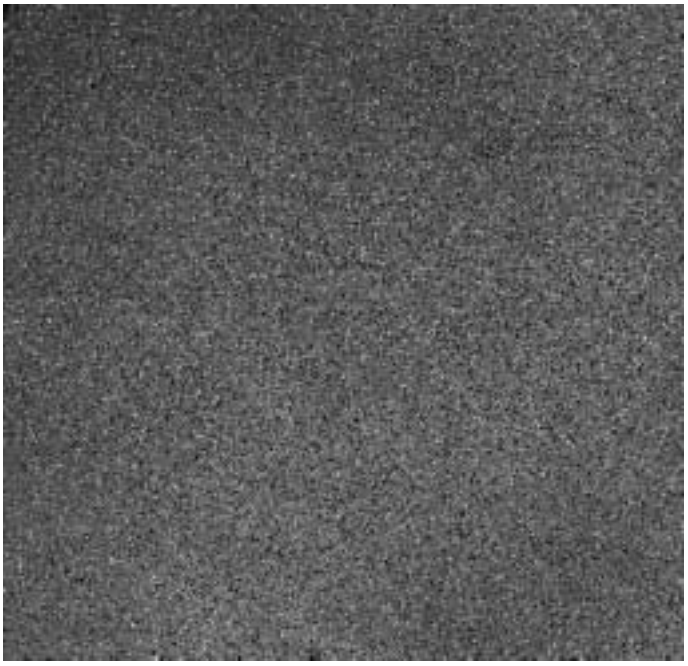

Figure 1: Image of a SPARS200 dark map. Dark points are masked pixels.

In the following sections, each SMS shall be discussed in detail. In all analysis below, we follow the detector orientation convention used by Robberto et al. (2002), with quadrant 1 located in the lower left quarter of the detector, and quadrant numbers increasing in the clockwise direction.

3.1 IR01S02 - Dark Current at Non-Nominal Temperatures

3.1.1 Test Description

The SMS IR01S02 was run three times during thermal vacuum testing. A single run consisted of one full frame IR ramp in STEP400 mode (exposure time of 2805 seconds), followed by a full frame ramp in RAPID mode (exposure time of 67 seconds). The goal of this test was to monitor the dark current level at various temperatures. During the first two runs of the SMS, the detector was held at the nominal operating temperature of -123^{o}C.

For the third run, the temperature was decreased to -127°C, the coldest operating temperature that could be maintained by the TECs.

Temp (°C)	Sample Sequence	Detector Median / Standard Deviation of Dark Current (e^-/sec/pix)
-123	RAPID	0.251 / 0.510
	RAPID	0.248 / 0.339
	STEP400	0.134 / 0.060
	STEP400	0.133 / 0.060
-127	RAPID	0.147 / 0.307
	STEP400	0.112 / 0.038

Table 2. Median dark current rates and corresponding standard deviations at nominal and non-nominal operating temperatures. The reported uncertainties are the standard deviation of the dark current values in all unmasked pixels of the indicated detector area.

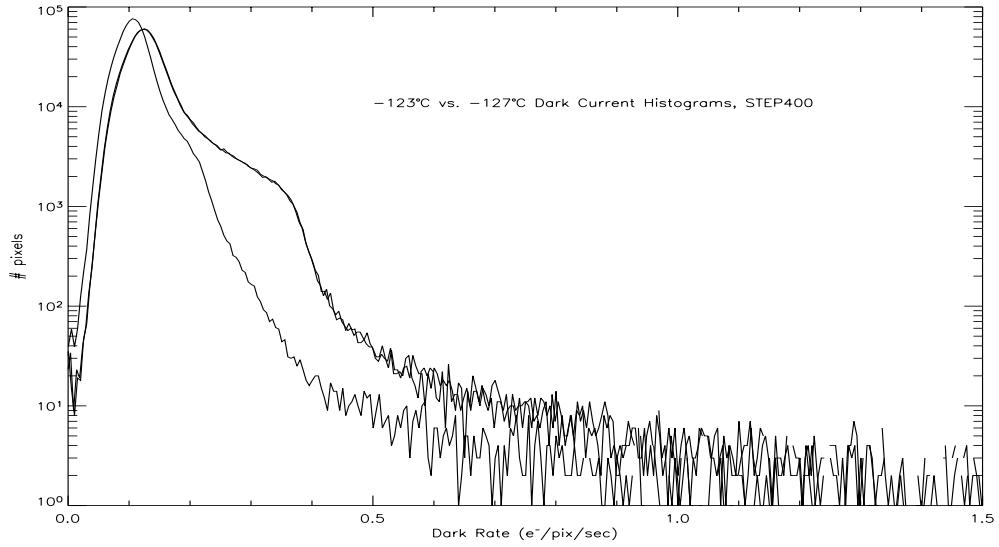

Figure 2: Histograms of the three STEP400 dark maps in IR01S02 testing. The two histograms with higher dark current tail show the dark current at an FPA temperature of -123°C, while the histogram that is shifted to lower dark currents is from data taken with the FPA at -127°C. The high dark current tail (> 0.5 e^-/sec/pix) is the result of applying an "out-of-date" mask, created from data taken 20 days prior to the IR01S02 data. This effect is more thoroughly investigated in the IR01S03 test.

The median dark current value for each dark current map is shown in Table 2. Medians were computed using all unmasked pixels in the dark current maps. The spread of the dark current was computed by calculating the standard deviations of the dark current maps. The three corresponding histograms for the STEP400 dark maps are shown in Figure 2.

Measured dark current rates were affected by three characteristics.

3.1.2 Temperature Variations

When the FPA temperature decreased from -123^{o}C to -127^{o}C, the median dark current decreased by 40% when measured from the RAPID ramps, and by 15% when measured from the STEP400 ramps.

3.1.3 Differences in Exposure Time

In the initial minute of the long STEP400 ramps, the dark rates were comparable (slightly lower) to those measured in the shorter RAPID ramps (Figure 4). Over longer timescales however, the STEP400 ramps exhibited lower average dark currents with cyclical modulations (Figure 3). Only during the phase of the cyclical variation with the highest dark current, such as between 1200 and 1600 seconds in Figure 3, the dark current measured with the STEP400 sample sequence matched that from the RAPID ramps.

3.1.4 Persistence and Crosstalk

Image persistence and crosstalk were also observed in all three iterations of this test. Latent images of the point sources used in the IR crosstalk tests (SMSs IR23S01 and IR23S02, 100X saturation illumination) performed nearly 7 hours before, were still visible at the same positions on the detector. We investigated the magnitudes of these extra signals in the IR01S02 frames by treating them as locally elevated dark currents.

In the first STEP400 ramp, the strongest persistence source had a “dark current” roughly 2.6 times greater than the median dark rate reported in Table 2. In the final STEP400 file (acquired at an FPA temperature of -127^{o}C), the signal associated with this source had decreased to roughly 40% above the median dark rate. In both cases, the persistence and crosstalk sources do not affect the median dark rates reported in Table 2, because of the small number of pixels affected.

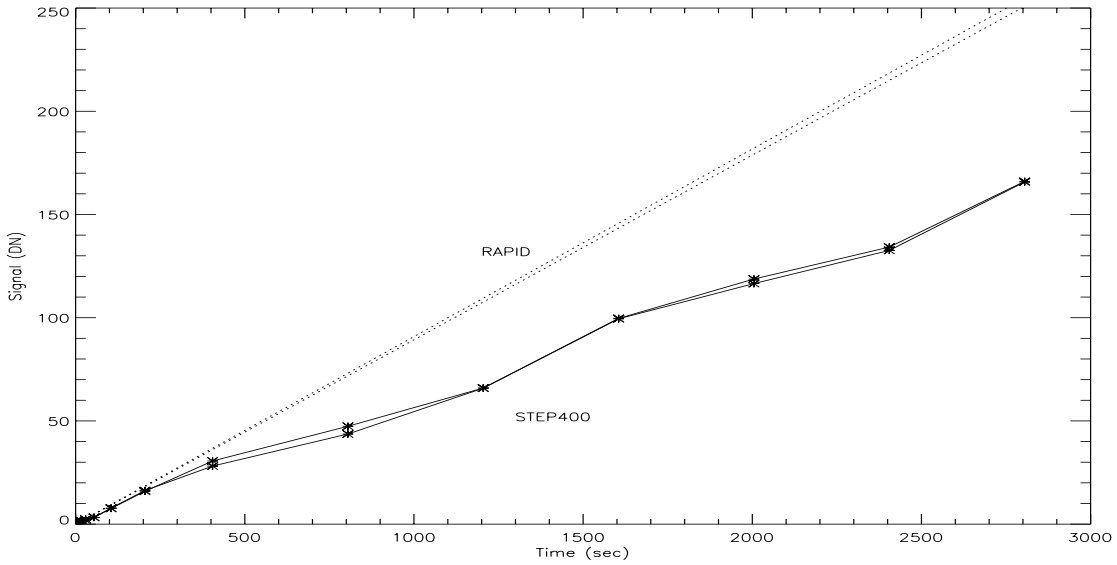

Figure 3: Median signal in 200 by 200 pixel boxes for the RAPID and STEP400 ramps taken at -123^{o}C. In this case, the lines marked 'RAPID' are best-fit lines to the RAPID data, extrapolated to the timescale associated with the STEP400 data. Note the cyclical modulation of the dark current in the STEP400 data, associated with FPA temperature variations.

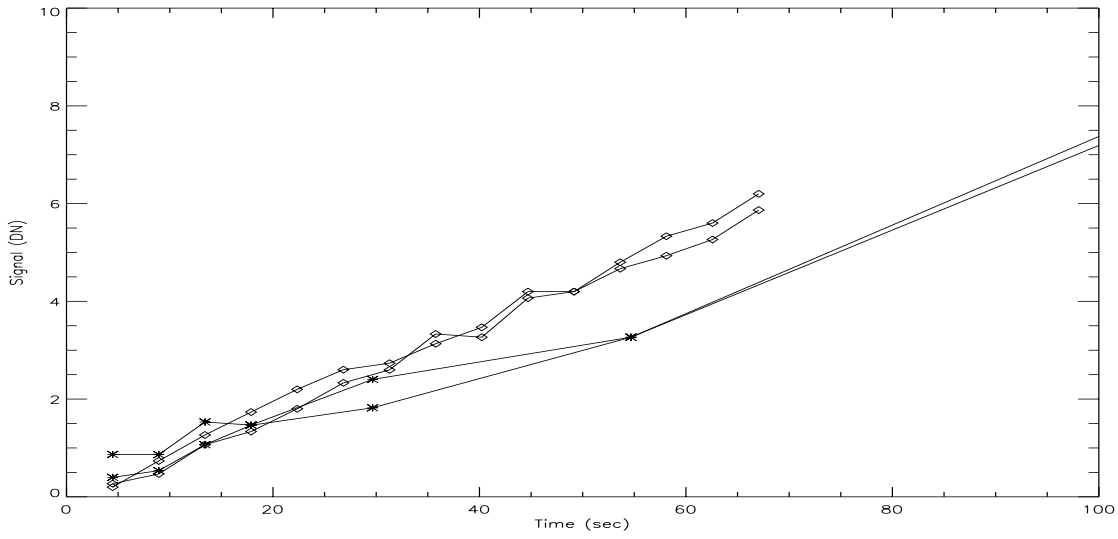

Figure 4: Median signal in 200 by 200 pixel boxes for the RAPID ramps and first 6 reads of the STEP400 ramps, taken at -123^{o}C. The RAPID ramps, which are 67 seconds long, show a constant dark rate, which is higher than the dark rate in the initial ~55 seconds of the STEP400 ramps.

3.2 IR01S03 - Dark Current for RAPID and SPARS Sample Sequences

This SMS was developed to characterize the dark rate for the RAPID and SPARS sample sequences, which sample the detector signal at regular intervals. Over the course of thermal vacuum testing, this SMS was run 4 times, on days 251, 262, and twice on day 267 (September 7, 18, and 23, 2004, respectively). The SMS was aborted prematurely during both runs on day 267, so only the early files within the SMS were taken 4 times, while later files were taken twice. The data taken on day 251 were collected shortly after WFC3 came out of safe mode, which causes a change of FPA64 temperature and offset voltages. These disruptions typically have an adverse effect on the detector performance. We will actually see that the dark current data for day 251 exhibit inconsistent behavior.

3.2.1 Masking

With the large amount of data associated with IR01S03, ramps from this test were used to create mask files, which were applied to all IR01 data, to eliminate bad pixels.

Subsequent to the data reduction performed as described in the previous section, the stability of the hot pixel population was studied through the analysis of the hot pixel masks. Two masks were created from the SPARS200 exposures taken on day 251 and 262 using the technique outlined in Hilbert et al. (2003) Another mask was created from SPARS25 data taken on 267. The two masks created from the SPARS200 data each had ~85,000 pixels (8.3%) flagged as bad. The day 267 SPARS25 mask contained ~60,000 bad pixels (5.9%). In each case, ‘bad’ pixels were composed mainly (> 92%) of hot pixels. In comparing the three masks, spanning a range of 16 days, 90.9% (~935,000) of the pixels in FPA64 remain good in all three masks, while 5.4% (~56,000) of all pixels are hot in all three masks. The remaining 3.7% of pixels are hot in one or two out of the three masks. The effect of this changing population of bad pixels on masked data is shown in Figure 5. The high dark current tail of a day 251 file is well masked when the maskfile is created from day 251 data. A maskfile created from day 262 data however, fails to remove a large portion of the day 251 hot pixels. As a result of the change in hot pixel population, ramps in all tests were masked with mask files created from data taken close in time.

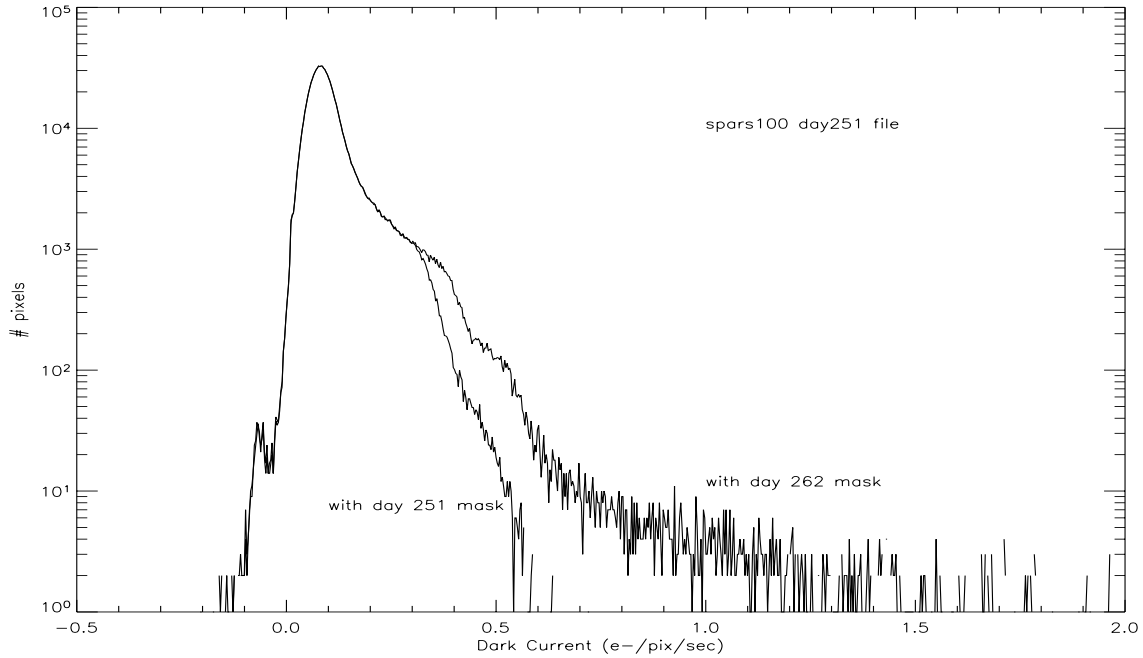

Figure 5: Histograms of a dark current map for a day 251 SPARS100 (1405 second exposure time) file. The histogram with the dark current tail results when the mask applied comes from day 262 data, while the mask created from day 251 data eliminates the high dark tail. This suggests a population of high dark current pixels that changes on the timescale of days.

3.2.2 Dark Rates

Once each ramp was masked, a dark current map was created by fitting a line to the signal in each pixel over time, as described for the IR01S02 test. As a consistency check across the multiple runs of this SMS, the median dark current rate for each ramp was calculated. A subset of the results is shown in Table 3, with typical dark currents, for longer sample sequences, of ~0.14 e^-/sec/pix. A number of anomalies were also apparent in this SMS.

Repeated SPARS25 ramps for day 251 show a dark current that is decreasing with time. In particular, the dark current rate in the third SPARS25 ramp is lower than that measured on subsequent days by almost a factor of three. The same phenomenon also appears in the third RAPID file on day 251, the third SPARS25 file for day 262, and the day 251 SPARS100 data, where the dark current remains below that seen in all subsequent data. Given the odd behavior of the dark current in most of the day 251 data, these files were ignored in subsequent analysis.

.

Day	Median Dark Current (e-/sec/pix)	Uncertainty (Standard Deviation) (e-/sec/pix)	Day	Median Dark Current (e^-/sec/pix)	Uncertainty (Standard Deviation) (e^-/sec/pix)
	RAPID			**SPARS25**	
251	0.245	0.304	251	0.213	0.092
	0.243	0.305		0.175	0.099
	0.081	0.304		0.058	0.091
262	0.241	0.306	262	0.148	0.089
	0.208	0.304		0.151	0.089
	0.201	0.308		0.110	0.088
267	0.189	0.313	267	0.137	0.100
	0.217	0.307		0.140	0.100
	0.187	0.309		0.152	0.100
	0.218	0.308		0.148	0.100
	0.189	0.307		0.140	0.099
	0.178	0.308		0.145	0.099
	SPARS100			**SPARS200**	
251	0.099	2.486	251	0.129	1.646
	0.098	2.497		0.140	1.651
	0.097	2.491		0.145	0.057
262	0.127	0.061	262	0.137	0.054
	0.138	0.061		0.132	0.054
	0.137	0.061		0.136	0.054

Table 3. Median dark current values for maps created from individual ramps. Unexplained behavior is apparent in day 251 data for all but the SPARS200 ramps. As a result of this strange behavior, day 251 data was not used in the creation of median dark maps for each sample sequence.

The final processing step in this test was to create a median dark current map ("super-dark") for each sample sequence. The median dark current in each pixel was calculated from the set of individual ramps, ignoring the masked pixels, and the resulting image was saved. Histograms of these median dark maps were then calculated and are shown in Fig-

ures 6 and 7. The median dark currents in these median dark current maps are shown in Table 4, together with the standard deviation of the image.

Sample Sequence	**Detector Median / Standard Deviation of Dark Current (e^-/sec/pix)**
RAPID	0.200 / 0.152
SPARS10	0.166 / 0.010
SPARS25	0.137 / 0.085
SPARS50	0.151 / 0.067
SPARS100	0.133 / 0.059
SPARS200	0.135 / 0.054

Table 4. Median values of the median dark current maps for the FPA64, for the RAPID and SPARS sample sequences. The CEI Specification for IR channel dark current is 0.4 e^-/sec/pix.

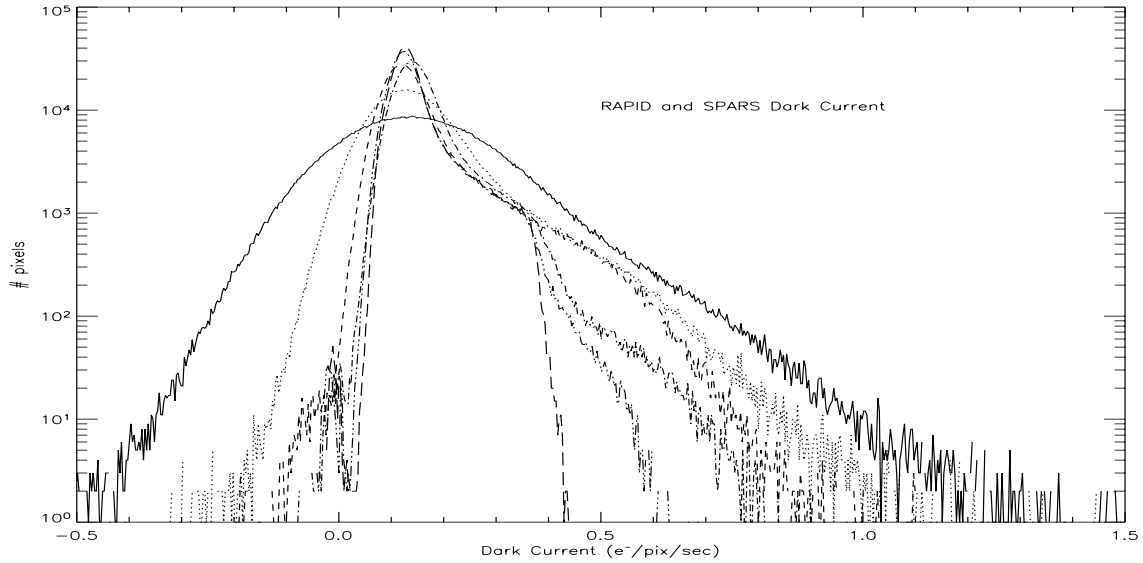

Figure 6: Histograms of the RAPID and SPARS sample sequence dark current files. The RAPID histogram is the solid line, with the widest peak. As exposure time increases with the SPARS sequences, the histograms become more narrow and sharply peaked. Also, the tail of high dark current pixels becomes smaller with increasing exposure time. Results from further investigation into this behavior will be addressed in a future ISR. The longest exposure (SPARS200, dashed line) shows no pixels, after masking, with a dark current greater than about 0.44 e^-/sec/pix. These histograms were created using the median dark current maps for each sample sequence, using only the day 262 and 267 data.

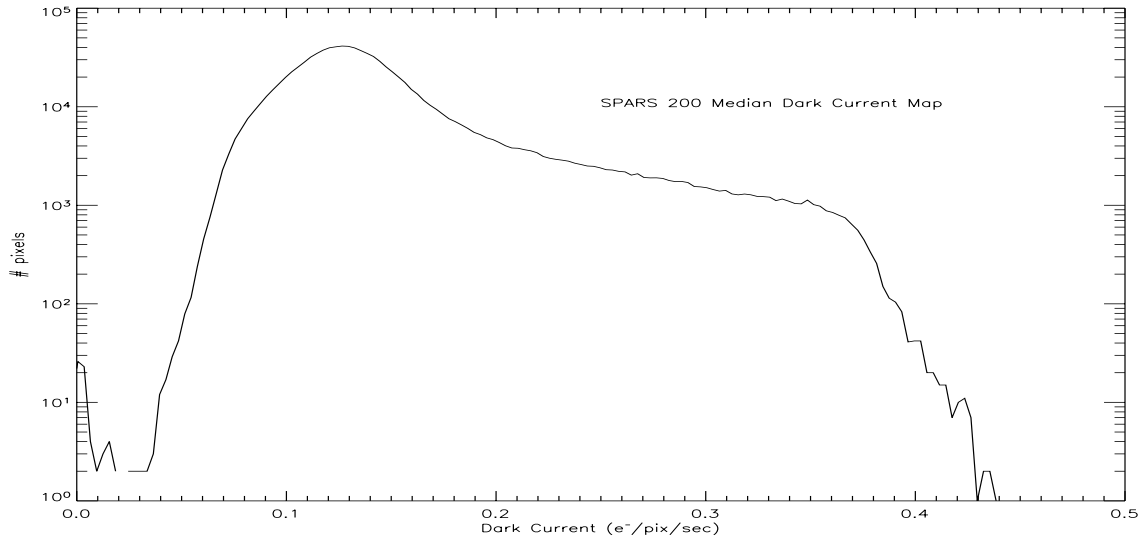

Figure 7: Histogram of the SPARS200 (2805 second exposure time) median dark current map, created from day 262 data.

Significant variations in the dark rate within ramps, similar to those observed in IR01S02, were also observed in these data. Figures 8 and 9 show the signal in the RAPID and SPARS100, day 262 ramps. As in Figures 2 and 3, the RAPID ramps show higher and more consistent dark current (steeper slope), while the SPARS100 ramps vary significantly, giving a broad range of dark current values.

An interesting feature of these SPARS100 ramps is the measured signal in the first 2 reads. In several of these long duration ramps the signal in the first two reads is nearly flat, corresponding to a very small dark rate. The dark rate then increases only after the second read. This anomalously small dark current between the two initial reads of a ramp is a small effect compared to the temperature dependent changes in dark rate seen in Figure 9, but nevertheless affects the line-fitting and calculation of the final dark rate.

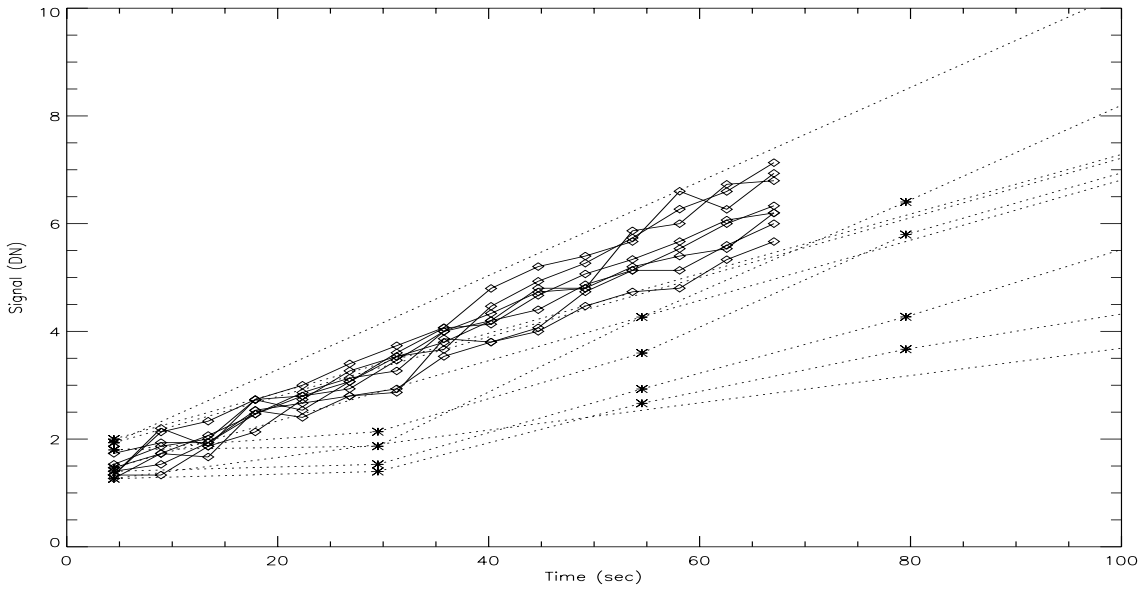

Figure 8: Median signals in a 200 by 200 pixel box. Diamonds: RAPID ramps; Asterisks: first 100 seconds of SPARS100 ramps.

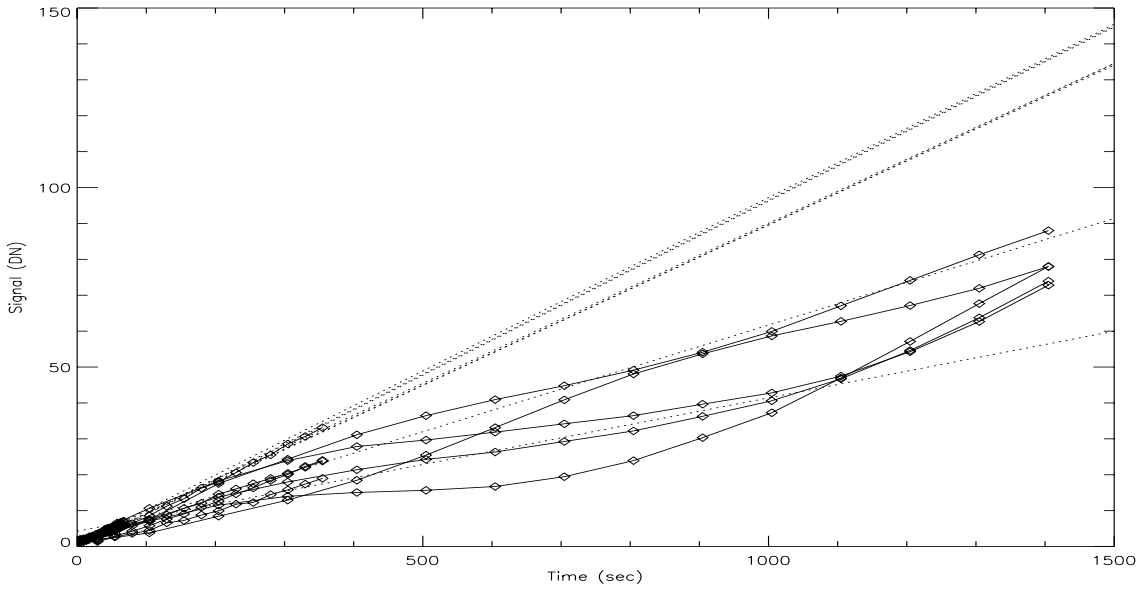

Figure 9: Same as Figure 8, but with the time scale expanded to show the full SPARS100 ramps (indicated by diamonds in this plot). The dotted lines are best-fit lines to the RAPID signal, extended to the SPARS100 timescale for comparison. Most of the RAPID ramps exhibit higher, and much more stable, dark current than the SPARS100 ramps.

3.2.3 Thermal Effects

Even with the IR01S03 ramps all taken at the same nominal temperature of 150K, we found evidence for dark current variations correlated with small fluctuations of the detector temperature. In Figures 10 and 11, we show the dark rate plotted along with the FPA temperature for each of the SPARS50 and SPARS200 ramps taken in IR01S03. The duration of the SPARS50 ramps (~700 sec) is less than the period (~1500 sec) of the dark current variation seen in Figure 11, and therefore the relationship between temperature and dark current is unclear. However, the longer period of the SPARS200 ramps provides a clear view of the temperature/dark current relationship. The plots in Figure 11 show that the dark current oscillates with the same period as the detector temperature fluctuations, and a phase which lags that of the FPA temperature by about 1000 - 1300 seconds. The dark current within a ramp can vary by as much as 60% - 70% above and below the mean value, against a temperature change of only 0.3^{o}C. This small detector temperature variation cannot induce such a large change of dark current. This behavior may be present in all ramps, regardless of sample sequence, but only the longer sample sequences, such as SPARS100 and SPARS200, have timescales long enough that the temperature/dark current relationship can be easily seen.

We found that the 6 stage thermoelectric cooler (TEC) voltage also varied cyclically during these tests. An increase of the TEC voltage corresponds to a decrease in FPA tem-

perature, suggesting that there is a delay between the thermal control loop and the detector temperature. Figure 12 illustrates the relationship between dark current and TEC voltage.

Spatial variations of the dark current levels were also found during this test. Median dark current at the edges of the detector was observed to be lower than that in the center by up to 10%. Figure 12 shows the differences in dark current between the center and edges of the detector. Further investigation into spatial dark current variations in FPA64 are summarized in the Conclusions.

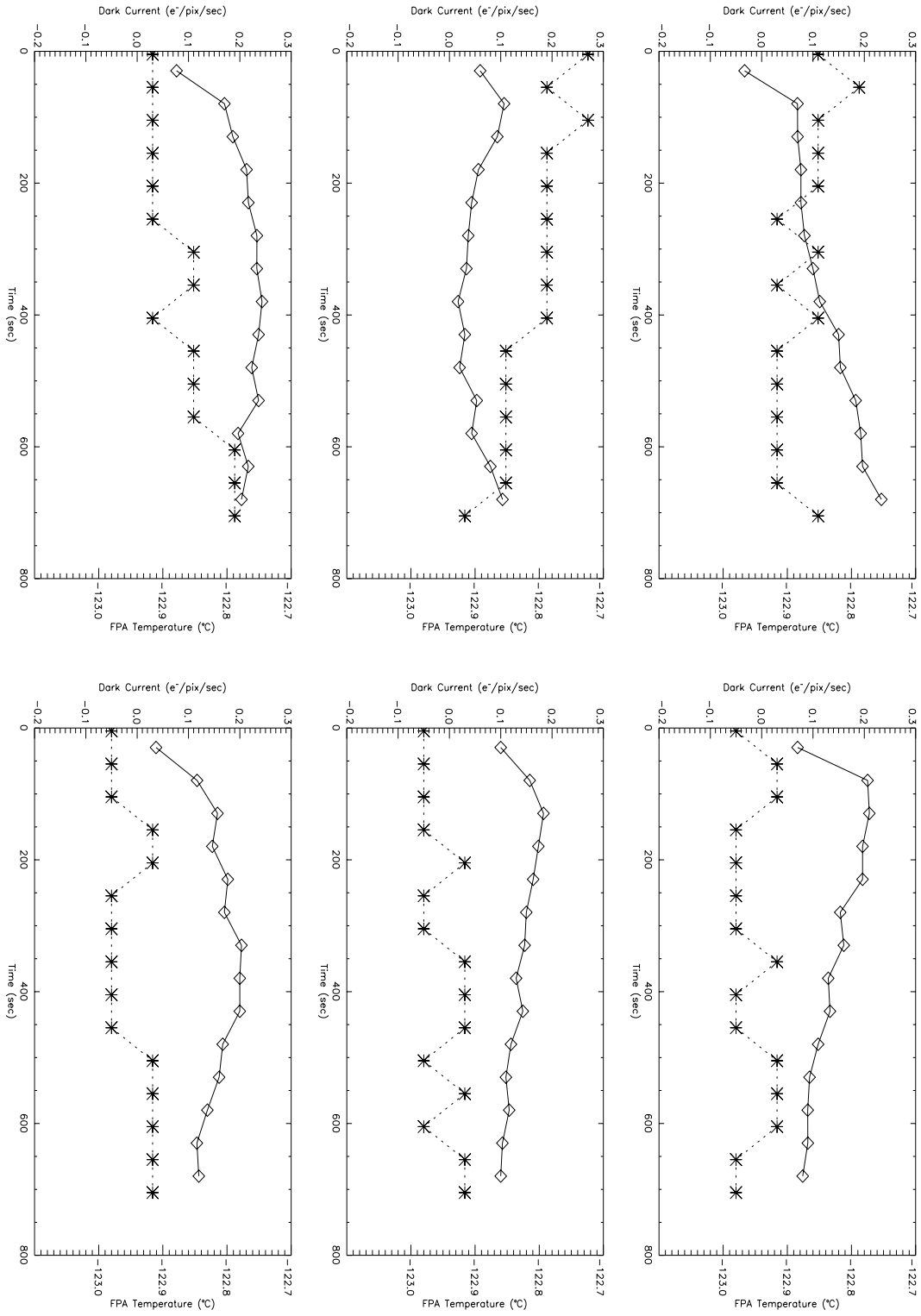

Figure 10: Signal rates and FPA64 temperatures for the SPARS50 files in IR01S03. Temperature values are shown with stars, while dark currents are shown with diamonds. The relationship between small temperature changes and dark rate is unclear.

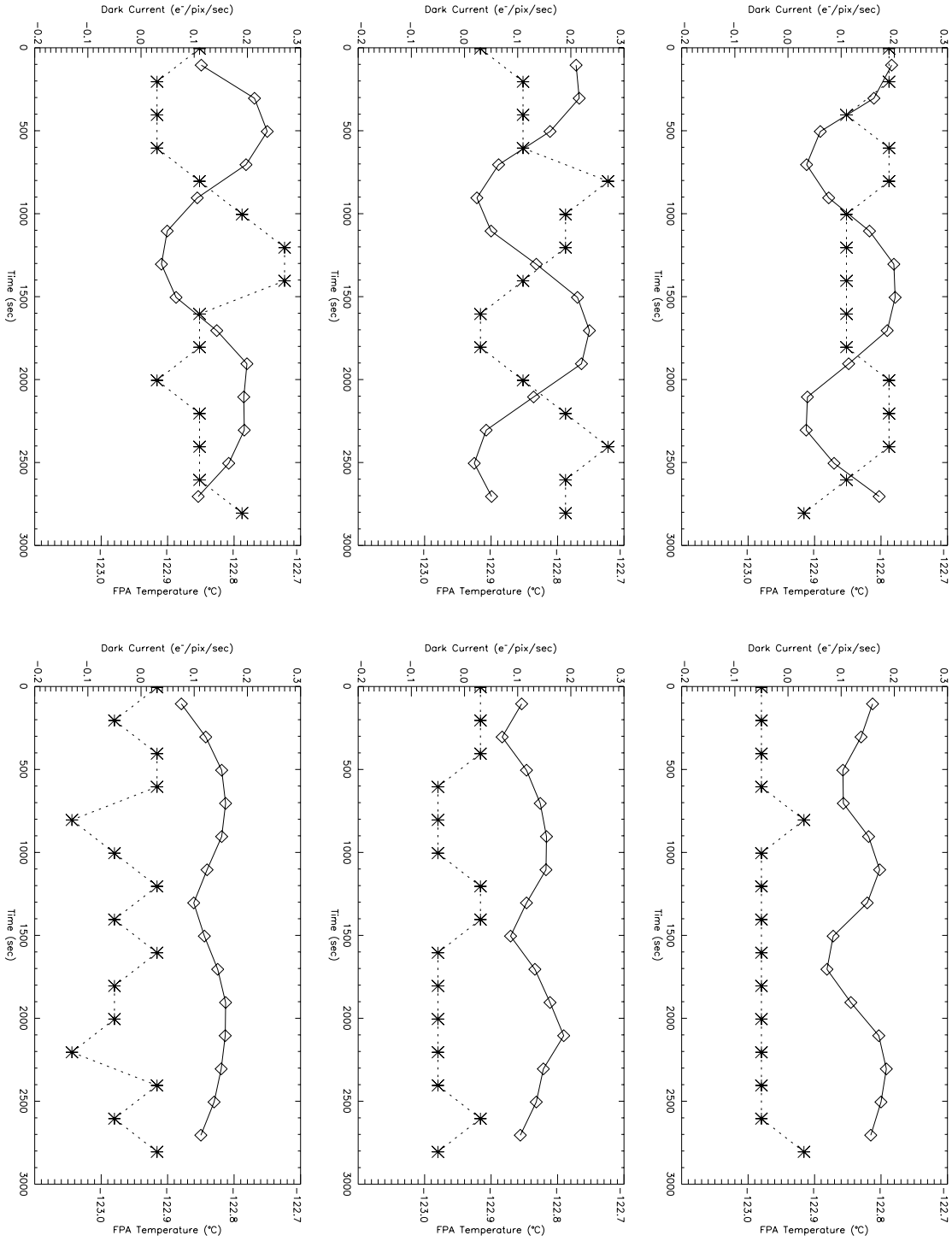

Figure 11: Signal rates and FPA64 temperatures for the SPARS200 ramps in IR01S03. Temperatures are shown with stars, and dark currents are shown with diamonds. The correlation between high temperature and low dark current is clear in these ramps.

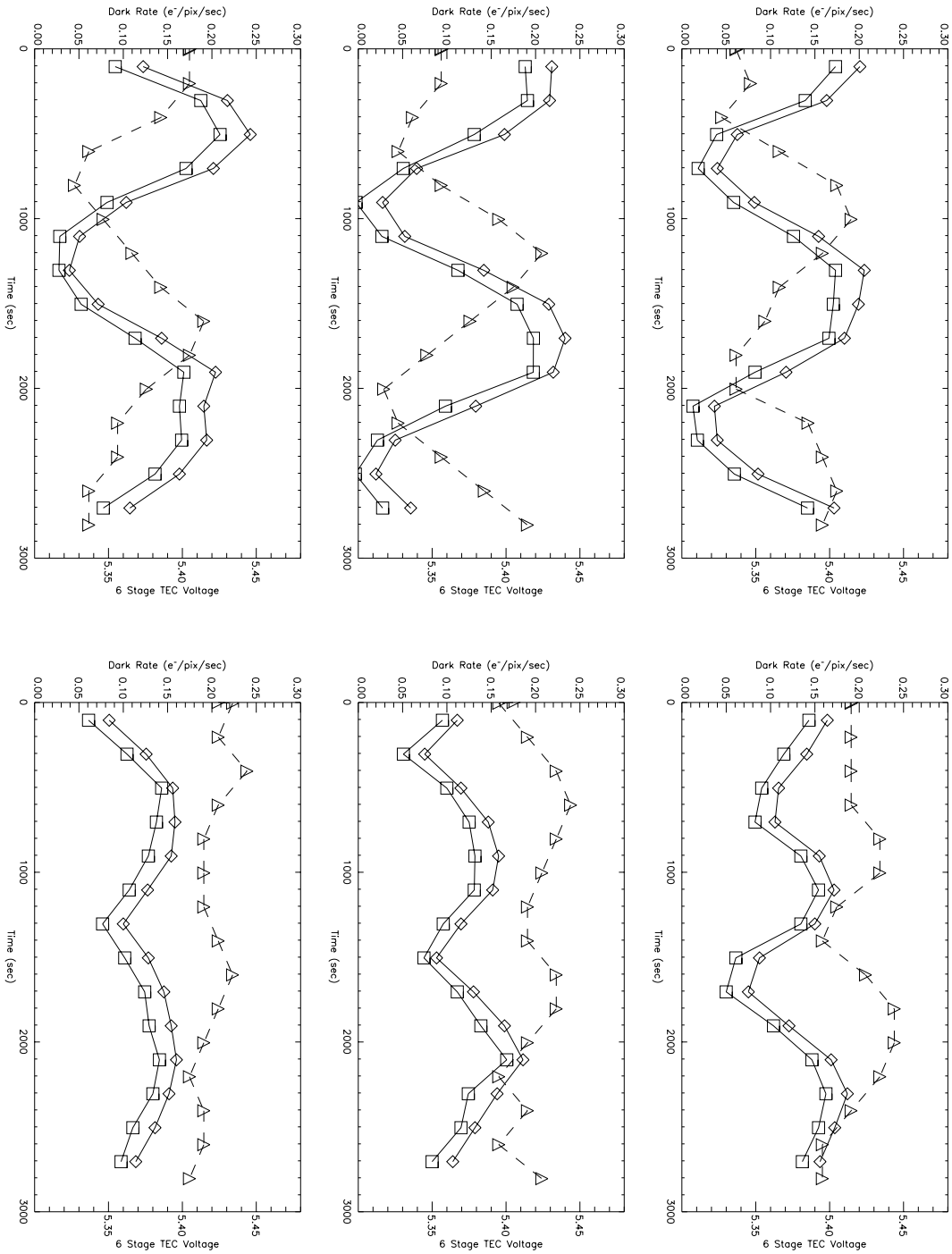

Figure 12: Dark rates and 6-stage TEC voltage levels for the SPARS200 files in IR01S03. The dashed line is the TEC voltage, while the solid line with diamonds shows the dark current in the corner of quadrant 3 at the center of the detector. The solid line with the squares shows the dark current in the upper left corner of quadrant 3 (towards the top center of the detector). This same situation, with higher dark current in the center of the detector compared to the edges, occurs in all quadrants.

3.3 IR01S04 - Dark Current for STEP Sample Sequences

This test, similar to IR01S03, was designed to generate dark current maps for the STEP sample sequences. Data reduction and analysis followed the same method outlined for IR01S03. The same inconsistent behavior seen in the day 251 data for IR01S03 was also observed in the day 252 data here. This is not unexpected, as the IR01S04 data were taken immediately after the IR01S03 data on days 251/252. Therefore, as with the IR01S03 data, only day 262 data of this SMS were used in the creation of median dark current maps for each sample sequence. The median dark current values for these sample sequences are shown in Table 5.

Sample Sequence	**Detector Median / Standard Deviation of Dark Current (e^-/sec/pix)**
STEP25	0.125 / 0.086
STEP50	0.145 / 0.072
STEP100	0.126 / 0.064
STEP200	0.139 / 0.059
STEP400	0.136 / 0.055

Table 5. Median dark current values for the STEP sample sequences.

The histograms for the median dark current maps appear similar to those produced in IR01S03. Figure 13 shows the dark current histogram for the STEP400 (2805 second exposure time) sample sequence. This histogram is nearly identical to that for SPARS200 (2805 second exposure time) shown in Figure 7.

Temperature effects similar to those seen in IR01S03 were also seen in this test. Plots of the dark current and temperature variations for the STEP400 ramps appeared very similar to those from the SPARS200 files in Figures 11 and 12.

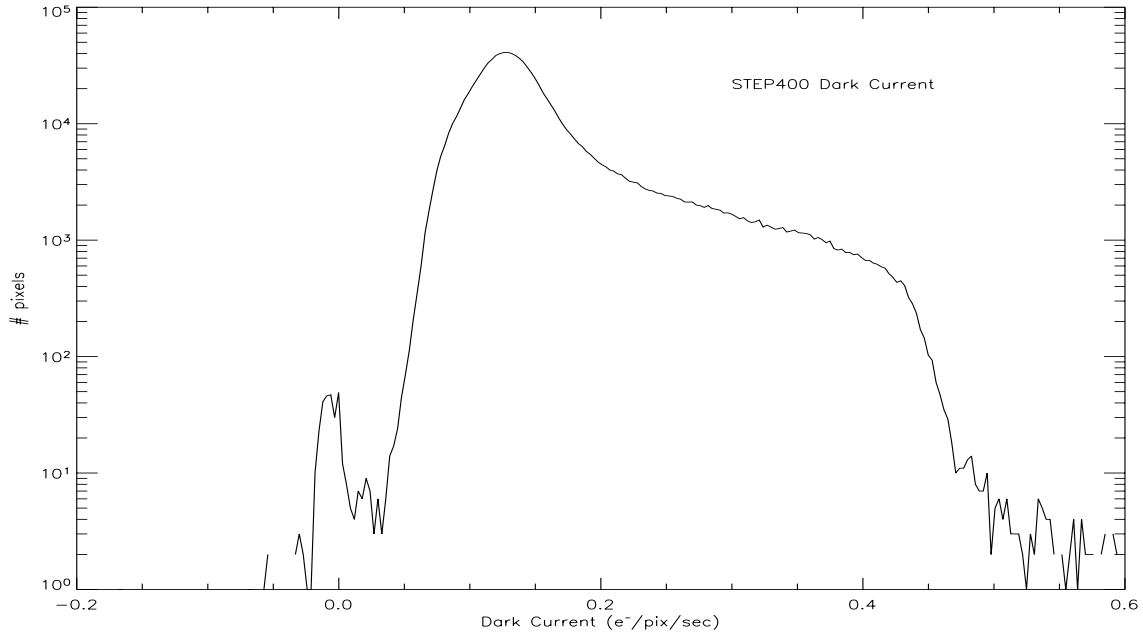

Figure 13: Histogram for the median STEP400 dark current map. This is the longest sample sequence, with a total exposure time of 2805 seconds. Note the similarity to the histogram for the median SPARS200 dark current map, in Figure 7. This indicates that the overall dark current behavior of FPA64 does not vary with the chosen sample sequence for sample sequences of similar total exposure duration.

3.4 IR01S05 - Dark Currents for MIF Sample Sequences

This test, similar to IR01S03 and IR01S04, was designed to generate dark current maps for the MIF sample sequences. Data reduction and analysis followed the method outlined for IR01S03 and IR01S04. Again, day 252 data provided inconsistent results, especially for the shorter sample sequences, and were ignored in creating the median dark maps. All data used in this analysis were taken on day 262, immediately after the IR01S03 and IR01S04 data. The median value of the median dark current maps are reported in Table 6.

The histograms for all MIF sample sequence dark current maps are shown in Figure 14. The exposure times for the MIF sample sequences only vary by a factor of 2.5 (600 through 1500 seconds), resulting in histograms with less variation than those created from the SPARS and STEP sample sequences. The high dark current tail, as with the other sample sequences, decreases with increasing exposure time. Overplotting the histograms of all MIF dark current maps shows the good stability of the FPA's dark current behavior over the course of the IR01S05 test.

Sample Sequence	Detector Median / Standard Deviation of Dark Current (e^-/sec/pix)
MIF600	0.137 / 0.066
MIF900	0.132 / 0.062
MIF1200	0.136 / 0.060
MIF1500	0.135 / 0.058

Table 6. Median dark current values, along with the standard deviation of the median dark current images, for the MIF sample sequences.

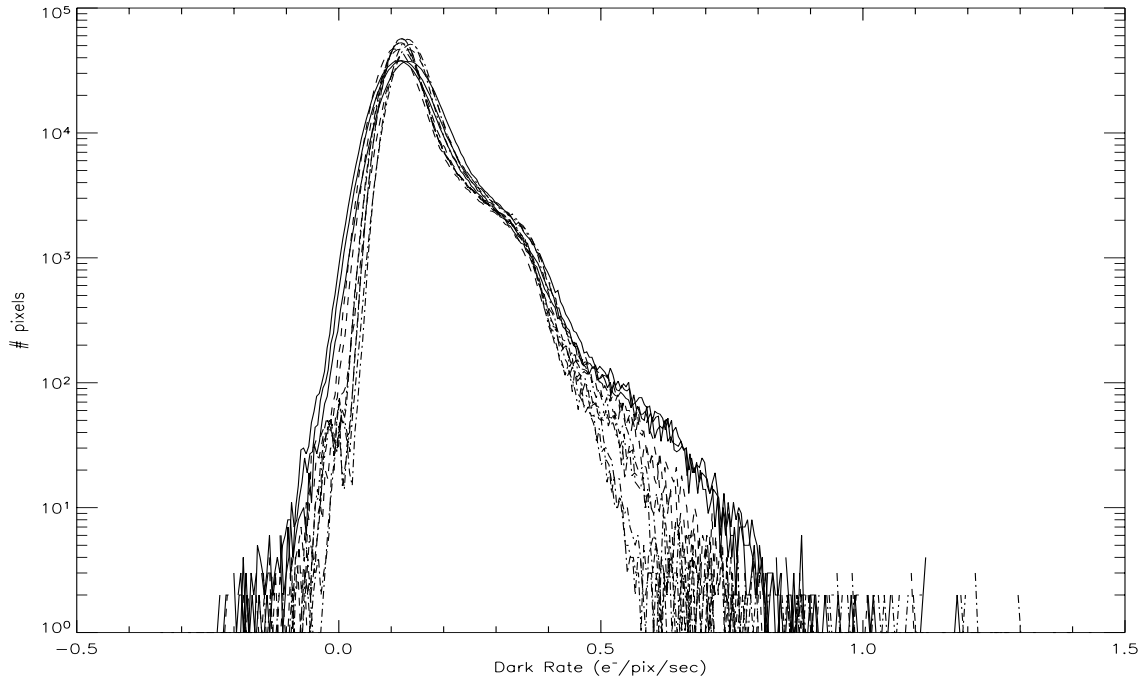

Figure 14: Histograms for all MIF sample sequence dark current maps (several histograms per MIF sample sequence). The histograms become slightly more narrow and higher peaked as exposure time increases. These histograms show the stability of the overall dark current behavior over the course of the IR01S05 test.

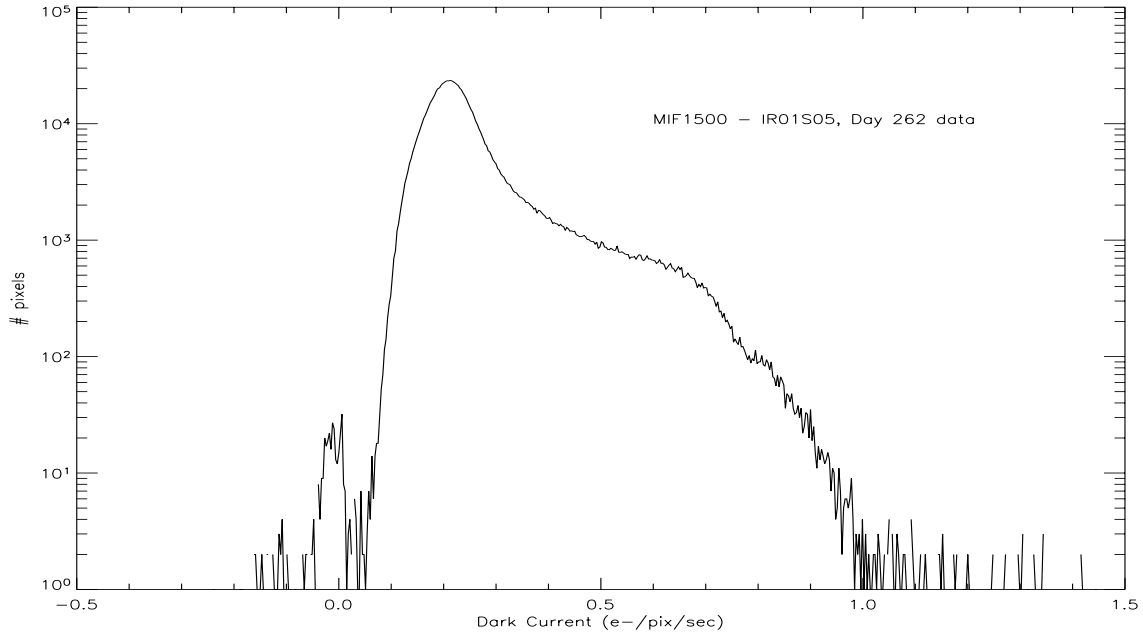

Figure 15: Histogram of the median MIF1500 (1500 second) dark current map.

3.5 IR01S06 - Dark Current VS. Cold Enclosure Temperature

This test was designed to examine the IR FPA's dark current levels as a function of cold enclosure temperature. The SMS was run twice during thermal vacuum testing, once on day 252, and once on day 260. The environmental conditions during the two iterations of the test were not identical. During the first run, the IR FPA temperature was held steady (within +/- 0.2^{o}C) at -123^{o}C, while the temperature of the cold enclosure was varied between -32.5^{o}C and -38.3^{o}C. Conversely, during the second run, the cold enclosure temperature was held steady at -35^{o}C, while the FPA temperature decreased from -122.9^{o}C to -126.2^{o}C.

Data reduction proceeded in the same manner as for the previous tests. A dark current map was produced from each data ramp, and the median dark current values from the maps were examined. All ramps in this test were taken with the SPARS100 sample sequence. Intra-ramp variations in the dark rate were observed in these ramps, just as in the IR01S03 test. However, since the duration of the SPARS100 ramps is roughly equal to one period of the cyclical detector temperature variation, the slope of a best-fit line, and therefore the calculated dark rate, is close to the actual dark rate averaged over a full period of detector temperature variations.

On the first run, the dark current decreased monotonically with cold enclosure temperature. However, when the cold enclosure temperature was raised from -38.3^{o}C to -35^{o}C at the end, the dark current remained stable at the level measured at -38.3^{o}C (Figure 16).

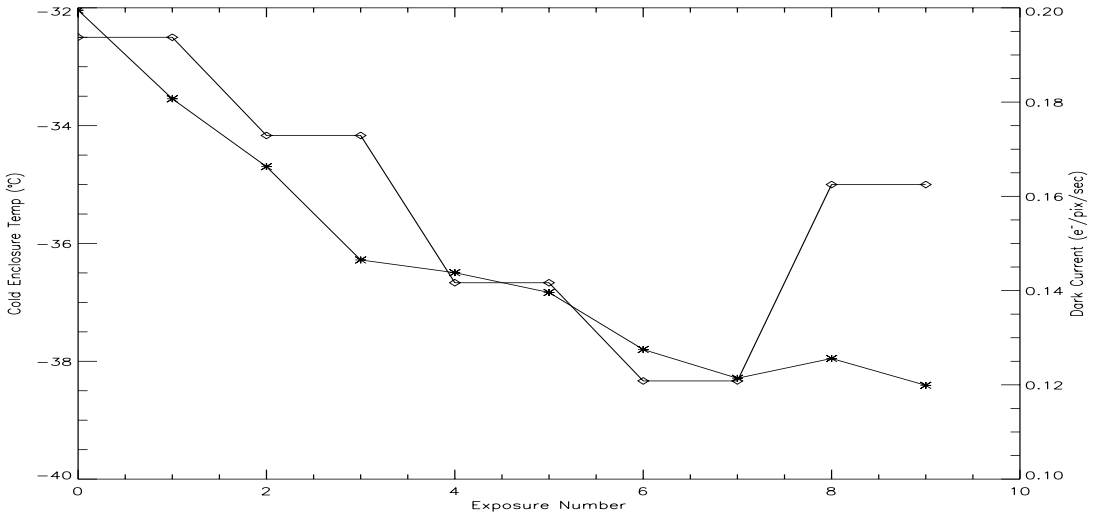

Figure 16: Cold enclosure temperature and median dark current for the data taken on day 252. The cold enclosure temperature is represented by the diamonds, while the dark current is shown with stars. The dark current decreases monotonically with the cold enclosure temperature, except at the end of the test, where the temperature is increased, and the dark current remains low.

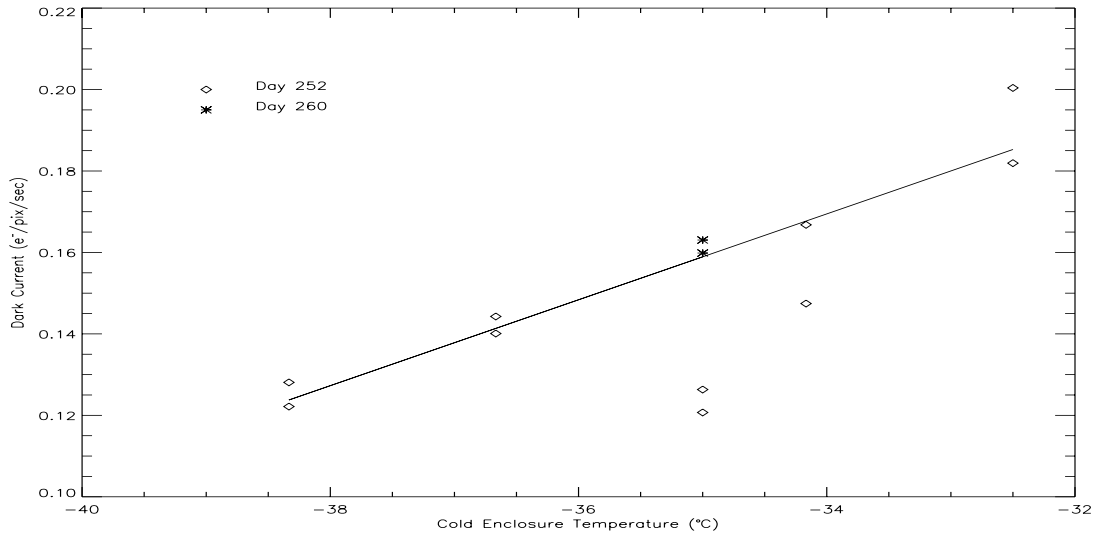

Figure 17: Median dark current versus cold enclosure temperature. The dark currents from day 260 fall in the position where one would expect the -35°C, day 252 values, suggesting that the thermal history of the cold enclosure may have had an effect on the day 252 dark rate. The two anomalously low data points at -35°C were excluded in the calculation of the best-fit line.

Ignoring the time at which data were taken, and simply plotting the dark current as a function of cold enclosure temperature, reveals more clearly the relationship between the two (Figure 17). The two low points at -35^{o}C are the final two files of the day 252 test, when the enclosure temperature was increased, but the dark current did not. The first two ramps taken on day 260 under the same instrumental conditions (detector temp: -123^{o}C, cold enclosure temp: -35^{o}C) provide an almost perfect match to the observed trend.

From the data points shown in Figure 17 (excluding the low dark current points at -35^{o}C), the dark current over the -32^{o}C to -37^{o}C cold enclosure temperature range follows the linear equation:

Dark current (e^{-}/sec/pix)= 0.530 + (CE Temperature (^{o}C)* 0.011)

The dark current behavior as a function of FPA temperature, measured during the second iteration of this test, is more complex. In general, the dark current decreases with decreasing FPA temperature, but there are seemingly anomalous cases, as can be seen in Figure 18. One of the observations taken with the FPA at -124.2^{o}C shows an extremely low dark current, while an observation made with the FPA at -126.2^{o}C shows a very high dark current compared to two other, identical observations. The inclusion of the two day 252 points taken under identical conditions seems to add scatter to the plot, but the STEP400 data from IR01S02 fall close to the day 252 points.

It must be said that the two ramps corresponding to the -124.2^{o}C points in Figure 18 were taken at different points in the detector temperature cycling. As Figure 19 shows, the point in Figure 18 with the higher dark current has been obtained with the detector temperature increasing over the course of the ramp, where the dark current is relatively stable, remaining between 0.13 and 0.19 e^{-}/sec/pix. For the point with the lower dark current however, the temperature was decreasing as the ramp progressed, and the dark current was increasing from 0.06 to 0.17 e^{-}/sec/pix. This suggests that the scatter in dark current in Figure 18 may be dominated by the temperature/dark current cyclical variations discussed in Section 3.2.3.

In conclusion, it appears that variations of the cold enclosure temperature by a few degrees has a well defined effect on the dark current of the IR channel. The dark current behavior resulting from variations of the much colder FPA temperature is much less predictable. This may not be surprising, as was seen in previous tests and is shown in Figure 18, even when the conditions within the instrument are supposed to be held constant, the median dark current can vary by large amounts (>30%).

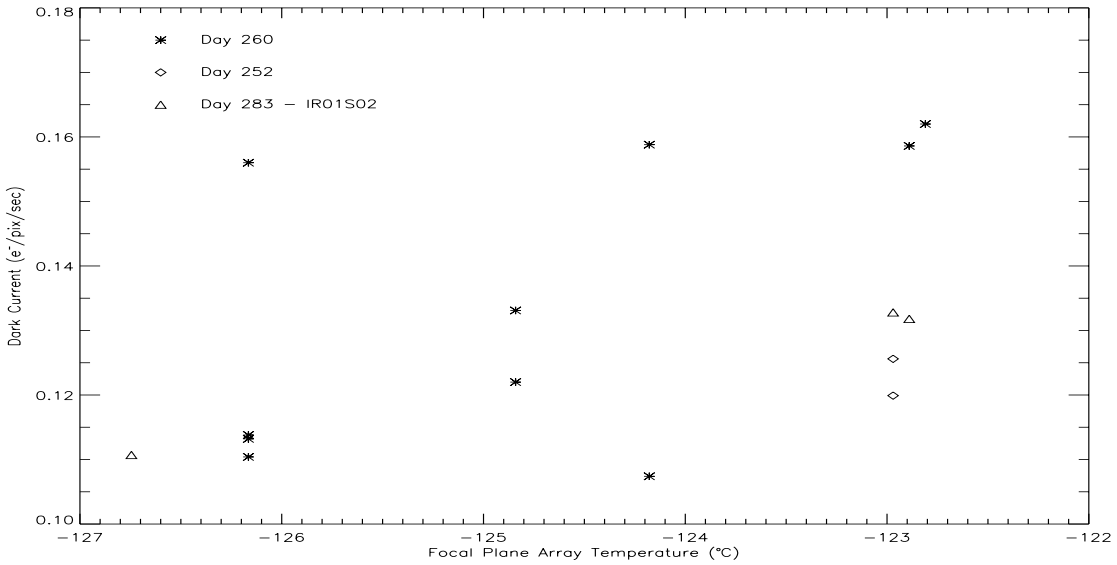

Figure 18: Median dark current as a function of FPA temperature. Dark current values from day 252 data as well as IR01S02 add to the scatter of the plot.

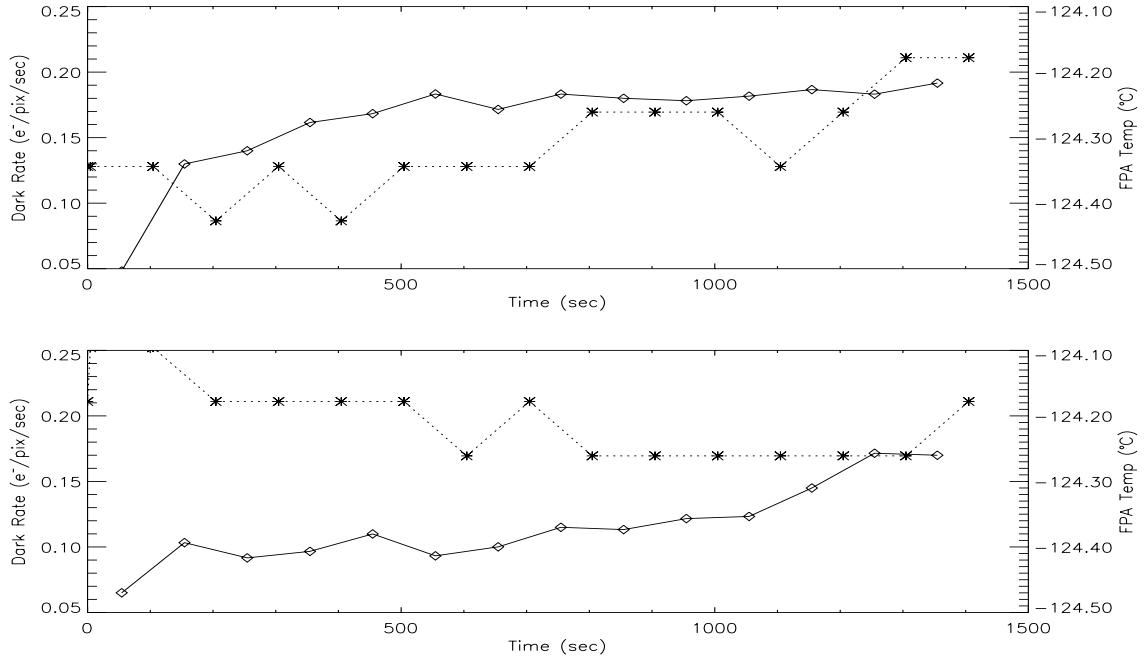

Figure 19: Dark current and FPA temperature up the ramp for the two points in Figure 18 at -124.2°C. Dark rate is shown with the solid line, while the dotted line denotes FPA temperature. The temperature varied by up to 0.33°C between the two ramps, leading to the ~0.05 e⁻/sec/pix difference in the reported median dark currents.

3.6 IR01S07 - Subarray Dark Current

SMS IR01S07 was designed to investigate the IR channel dark current in subarrays versus full-frame images. The SMS was run three times during thermal vacuum testing, resulting in the data files listed in Table 7. Data reduction proceeded following the same steps as the other dark current tests. A median dark current map was created for each sample sequence/subarray size file group. The median dark currents from these median dark current maps are also listed in Table 7. Subarrays are mostly intended for the photometric calibration of bright stars, and the relatively high dark current measured, in particular in the RAPID 64x64 mode, should not be a problem. The short overall exposure times for these data therefore made them unsuitable for looking at intra-ramp temperature and dark current variations.

Sample Sequence	Image Size (pixels)	# of File	Median Dark Current (e^-/sec/pix)	Standard Deviation (e^-/sec/pix)	Exposure Time per Image (sec)
RAPID	64 x 64	30	4.028	5.286	0.912
RAPID	256 x 256	30	0.512	0.563	10.16
RAPID	512 x 512	30	0.289	0.215	24.6
RAPID	1024 x 1024	15	0.177	0.128	67.0
SPARS10	512 x 512	30	0.149	0.098	102.4
SPARS10	1024 x 1024	15	0.144	0.094	144.9
STEP50	1024 x 1024	15	0.138	0.163	54.7

Table 7. Image sizes, median dark current, and standard deviation values for the IR01S07 data. The STEP50 data included only the first 6 reads of the sample sequence, resulting in the exposure time of 54.7 seconds, rather than the full STEP50 exposure time of 505 seconds.

3.7 IR01S08

IR01S08 was designed to look at the dark current through various IR filters, to check for extra thermal background signal admitted through the filters. The SMS was composed of 3-read, SPARS100 ramps (204 seconds exposure time), with the filter sequence DARK - FILTER - DARK - FILTER, etc., repeated while stepping through the filters in order of increasing central wavelength. Higher background signal was observed at the end through the F160W and grism filters, as seen in the 3 right-most peaks (time > 6000 seconds) of Figure 20. IR01S08's short ramps, when plotted chronologically, clearly reveal the variation of dark current with detector temperature. Figure 20 shows the dark current and detector temperature of FPA64 throughout the test. The cyclical variations of dark current

and detector temperature are evident in the figure. However, the variations are shown to be independent of the filter or blank (for dark frames) being used. Filled circles in Figure 20 represent data taken with the blank in place, resulting in a true dark frame. Open circles show the dark rate for data taken with a filter in place. The random distribution of filter and blank data in the peaks and valleys of the cyclical variation show that the dark current variations are not due to thermal background radiation reaching the detector through the filters.

Both the temperature and dark current cycle with a ~1500 second period during the test, with the dark current leading the detector temperature by ~300 seconds. The cause behind this behavior is unknown, as a 0.2^{o}C FPA temperature variation should not be enough to increase dark current by a factor of 10.

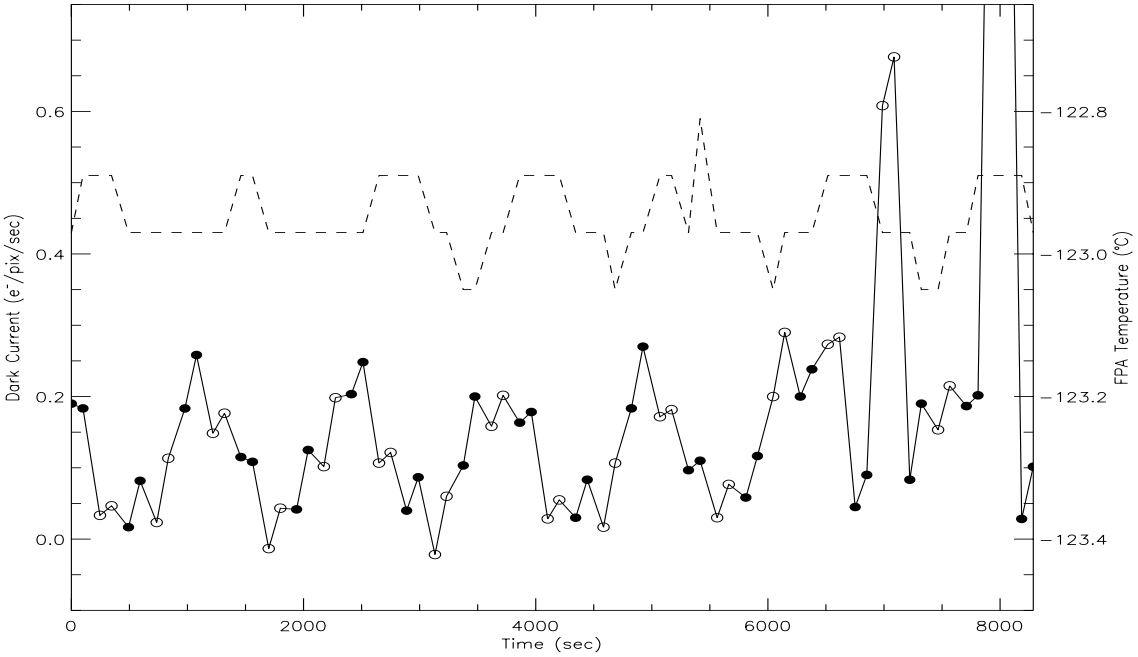

Figure 20: Dark current values (solid line) and FPA temperatures (dashed line) for the IR01S08 SMS. The dark current cyclical variation seems to lead the temperature variation by roughly 300 seconds. The elevated dark current values recorded after ~6000 seconds are due to increased background signal observed through the F160W filter and G102 and G141 grisms.

Data from IR01S08 were also used to search for temperature-related effects in the reference pixels of FPA64. Figure 21 shows the FPA temperature as well as the median reference pixel signal for the entire test. The reference pixels appear to roughly track the FPA temperature. From 3,000 seconds until the end of the test, the amplitude of the FPA temperature variation doubled to ~0.16^{o}C, and the reference pixel signal also varied

roughly with the same period. This tracking however, was not enough to correct for the increased dark current in the active pixels of the FPA, as seen in Figure 20. The bottom panel of Figure 21 shows the median dark current measured in quadrant 1 of FPA64, prior to reference pixel and zero-read subtraction. The correlation between dark current and detector temperature is less obvious in this case than when the data are reference pixel corrected.

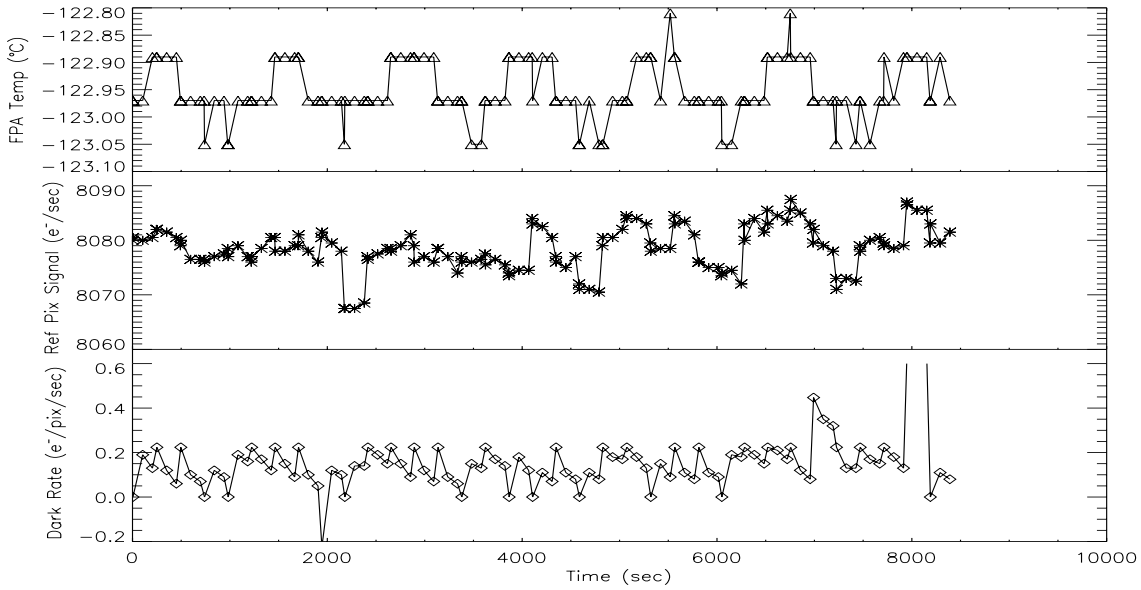

Figure 21: Science pixel dark current values (uncorrected by reference pixels), median reference pixel signals and FPA temperatures during the IR01S08 test. The reference pixels roughly tracked the temperature changes, especially as the amplitude of temperature variation increased.

Finally, a search was made for spatial variations of the dark current during the dark current cycling. A first median image was created from the images corresponding to the dark current peaks in Figure 20, and a second one was created from the images corresponding to the valleys. The difference of these two median images revealed a uniform image, with no discrete areas of greater or lesser average dark current variation. A histogram of the difference image, shown in Figure 22, shows that most pixels in the median peak image have a dark rate 0.22 e^-/sec/pix higher than in the median valley image. This seems to indicate that the dark current increase, which is apparently too large to be attributed to the variations of the measured detector temperature, also cannot be ascribed to enhanced radiative flux coming from the immediate vicinity of the detector.

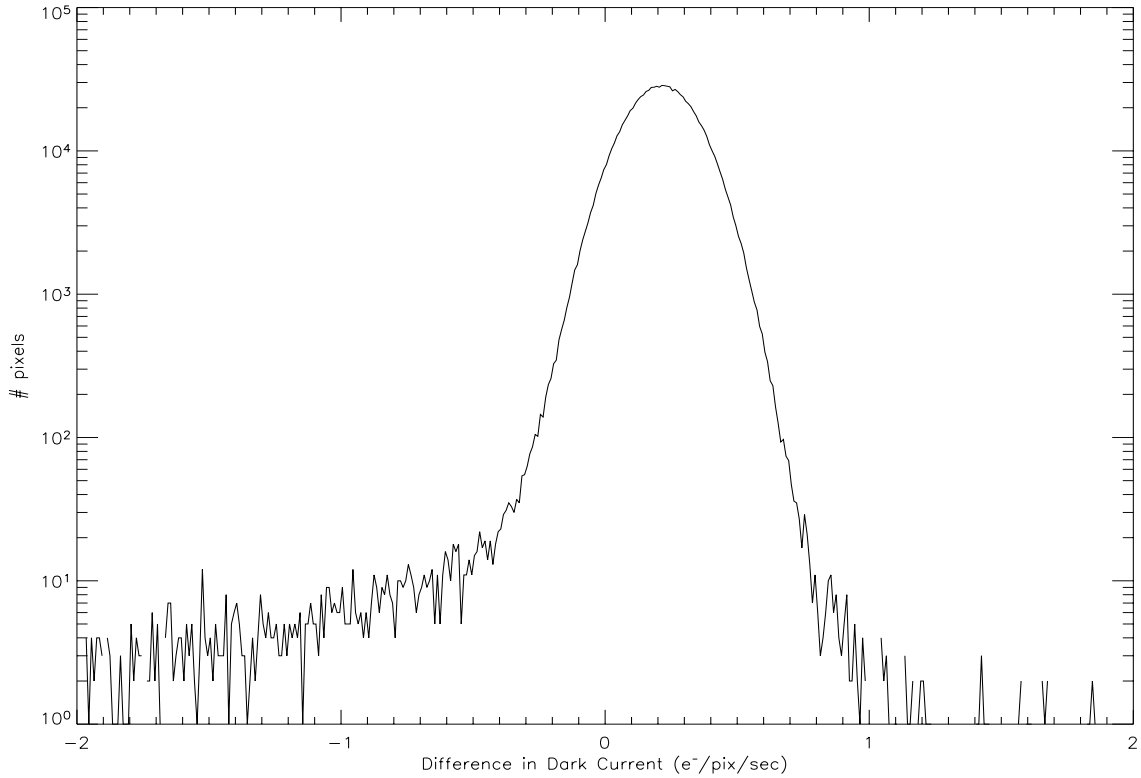

Figure 22: Histogram of the difference image between the median peak and median valley dark current from Figure 20. The mean difference in dark current is roughly 0.2 e-/sec/pix, as can be seen in Figure 20. There is also a small population of pixels with higher dark current during the low-FPA-temperature portions of the test. This is not surprising, given the large uncertainty associated with the 3-read ramps in this test.

3.8 IR01S09

The IR01S09 test was designed to test the functionality of the WFC3 IR thermo-electric coolers (TECs). The temperature in WFC3's heat pipes was raised, forcing the TECs to work harder in order to maintain the nominal FPA temperature. A series of 5- and 8-read SPARS50 ramps were taken during this heat transport testing. Figure 23 shows the FPA temperature and dark current during the test, similar to the plot for IR01S08 in Figure 20. In this case, the minimum temperature was 1.5^{o}C above the nominal operating temperature of 150K, and as the amount of heat at the detector became more than the TECs and heat pipes were able to carry away, the FPA temperature increased further by ~1^{o}C over ~13,000 seconds. Curiously, the overall measured dark current level remained stable over this temperature increase. All IR01S09 data were taken within a 4 hour window on day 291, far from any entries of WFC3 into safemode, implying that the IR01S09 data are free from the detector effects observed in the day 251 IR01S03 data.

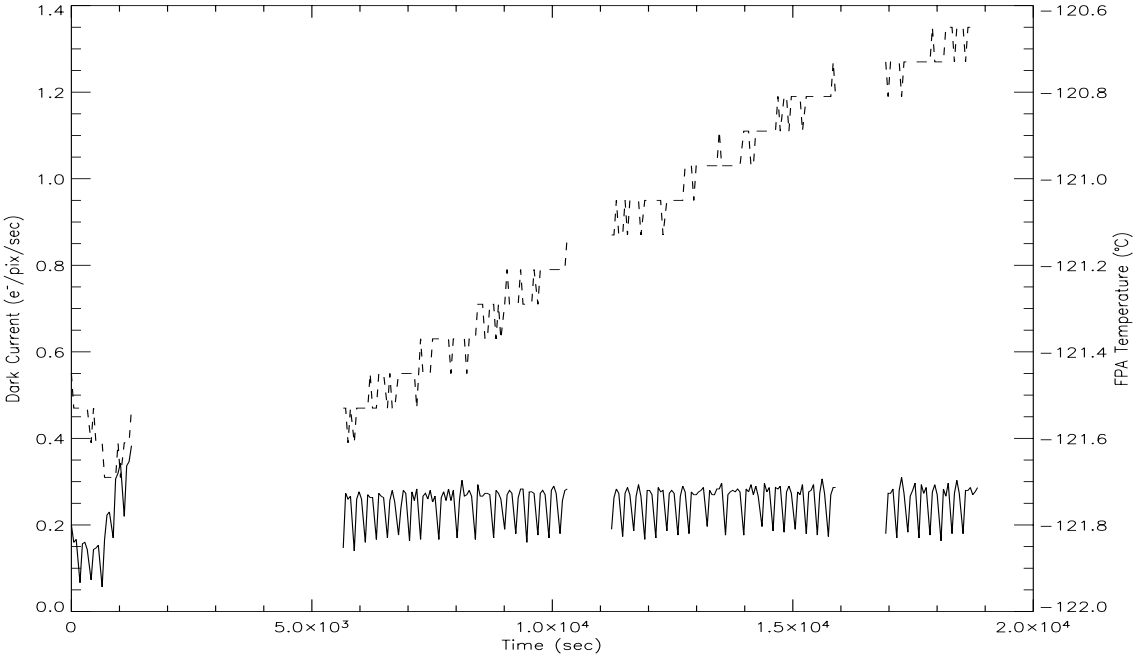

Figure 23: Dark current (solid line) and FPA temperature (dashed line) values during the IR01S09 test. Despite the increase in FPA temperature by nearly 1^{o}C, the dark current remained stable.

The IR01S09 ramps displayed the same anomalously low dark rate between the first and second reads as was noted in the IR01S02 data. After the second read however, the dark current remained relatively stable both within and among the ramps, as seen in Figure 24. With the limited number of reads in each ramp for these two tests, the low dark current in the initial read would have a large effect on the calculation of the final dark current map for each ramp. Ignoring the first read, the median dark current results are <0.005 e^-/sec/pix higher than when the first read is included. Characteristics of a subset of the IR01S09 data are shown in Table 8.

Detector Median / Standard Deviation of Dark Current (e^-/sec/pix)	FPA Temp: final read (^oC)	Cold Enclosure Temp (^oC)	6-Stage TEC Voltage (volts)
0.229 / 0.160	-121.13	-35.00	7.47
0.234 / 0.160	-121.13	-34.17	7.46
0.216 / 0.163	-121.53	-34.17	7.46
0.188 / 0.162	-121.53	-35.00	7.34
0.225 / 0.158	-121.53	-34.17	7.47
0.195 / 0.166	-121.61	-34.17	7.31
0.230 / 0.190	-121.73	-34.17	7.45
0.210 / 0.109	NA	NA	NA

Table 8. IR01S09 data characteristics, arranged in order of increasing FPA temperature. The median dark current varies by up to ~0.08 e-/sec/pix for ramps with identical FPA and cold enclosure temperatures. At the same time, two ramps with a 0.6^{o}C difference in FPA temperature can return nearly identical dark rates. This suggests a source for the dark current variation other than thermal effects from the changing FPA temperature. The bottom row gives median dark currents for a median image from all IR01S09 files. All data were taken on day 291, far from any instrument safemode effects.

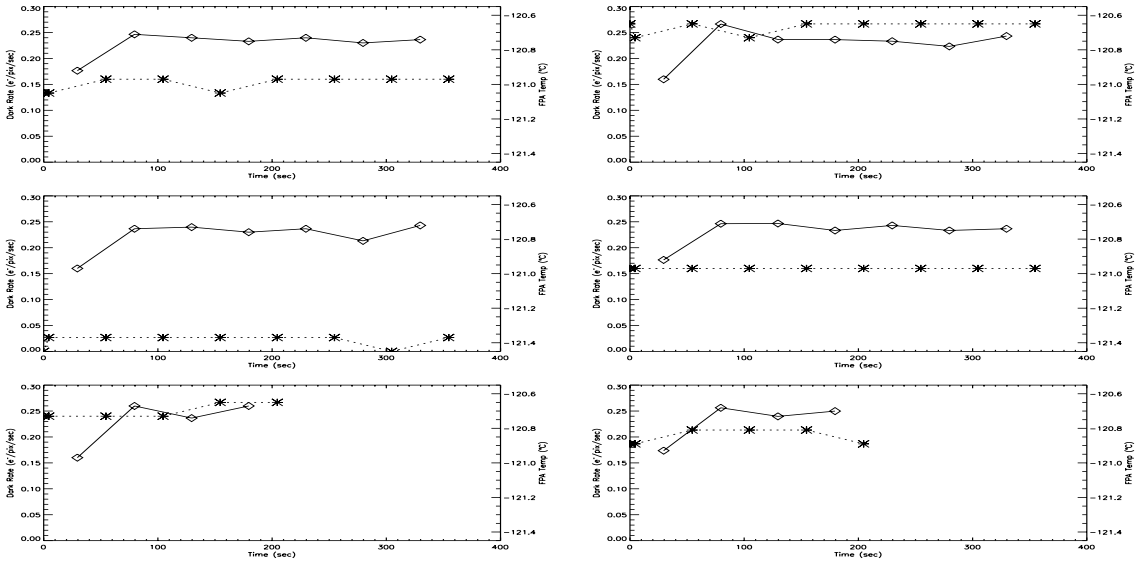

Figure 24: Intra-ramp dark rates and temperatures for 6 IR01S09 ramps. Minimal temperature variation within the ramps allowed the dark current to remain relatively stable. Note the low dark current in the first read of each ramp, as seen in IR01S02. Also note that the dark currents for all 6 ramps are nearly identical despite FPA temperatures which vary by 0.8^{o}C between ramps.

3.9 Manual Darks

In addition to the dark current ramps taken with pre-defined SMSs, 50 dark current observations were made on the fly during thermal vacuum testing. These data were reduced in the same manner as the data in the other dark current tests. A summary of the data characteristics is given in Table 9. Many of these manual dark current ramps were taken with fewer than the maximum number of reads per ramp. This resulted in observations with shorter exposure times and higher noise compared to ramps with the full number of reads per ramp in the previous SMSs. All manual dark current data were taken on days 266 and 267, and should be free from the instrument safemode effects present in the IR01S03 through IR01S05 data from days 251 and 252. We shall not discuss these data any further.

Sample Sequence	# files	# of Reads per Ramp	Detector Median / Standard Deviation of Dark Current (e^-/sec/pix)	Factor Increase in Uncertainty relative to 15 reads/ramp case
RAPID	10	4	0.282 / 0.477	15
STEP25	10	8	0.127 / 0.119	4
STEP100	10	10	0.128 / 0.088	2
STEP400	10	10	0.130 / 0.081	3
SPARS10	10	15	0.146 / 0.100	NA

Table 9. Median dark current values from medians of the ramps taken manually during thermal vacuum testing. All files are full-frame ramps, taken at nominal operating temperature. Uncertainties in the medians of the individual files were greater than those in previous tests for all but the SPARS10 files. This is because the full number of reads in the other sample sequences were not taken.

3.10 IR05S01

The IR05S01 test was created to measure the dark current in subarrays using two different sample sequences, RAPID and SPARS25. As with previous tests, a median image was created from each group of images with a given subarray size and sample sequence. The median dark current and uncertainty for each median image is reported in Table 10. These dark current values are in agreement with those reported for the subarrays in IR01S07, with one exception. The full frame RAPID image had a median dark current roughly 3 times larger than that in IR01S07. However, only two images were averaged in this case (as seen in the higher uncertainty value), while IR01S07 used 15 images.

Sample Sequence	Subarray Size (pixels)	Number of images	Median Dark Current (e^-/sec/pix)	Standard Deviation (e^-/sec/pix)
RAPID	64 x 64	8	4.447	8.805
	128 x 128	8	1.045	1.766
	256 x 256	8	0.534	4.689
	512 x 512	8	0.281	0.348
	1024 x 1024	2	0.535	1.775
STEP25	64 x 64	9	0.075	0.091
	128 x 128	5	0.132	0.094
	256 x 256	5	0.121	0.244
	512 x 512	5	0.146	0.092

Table 10. Median subarray dark current values for RAPID and STEP25 sample sequences. These dark rates match well with those measured for the subarrays in IR01S07, except for the full frame RAPID image. The 64 x 64 STEP25 image also has an anomalously low dark current.

3.11 IR04S01

The last dark current ramps we have examined as part of the TV dark current analysis came from the IR Linearity test, IR04S01. This test included 2 dark current ramps. The first was taken at the beginning of the test, in order to establish a baseline dark rate. The second dark was taken at the end of the test. Ten flat field ramps were taken between the two dark current ramps. These two darks, taken before and after detector illumination, were used to investigate persistence effects. Figure 25 shows the median signal in quadrant 1 of the detector for all reads of both dark ramps. Note the increased dark signal in the post-illumination ramp. This elevated signal decays as the ramp progresses, as seen by the change in the slope of the signal.

The median dark current in quadrant 1 of each read was calculated for both ramps. Figure 26 shows the difference in dark current behavior between the two ramps. The pre-illumination dark ramp exhibits a nearly constant dark current, at a level comparable with previously discussed full frame RAPID ramps.

The post-illumination ramp shows very different behavior, with a large dark current that decays over time. This dark rate is described by the exponential equation:

$$\text{Dark Current } (e^-/\text{sec/pix}) = 2.212 * 0.931^{\text{Time(sec)}} + 0.446$$

More data is needed to fully explore persistence effects, as the dark current decay equation above may be dependent on factors such as illumination levels, and time since the end of illumination.

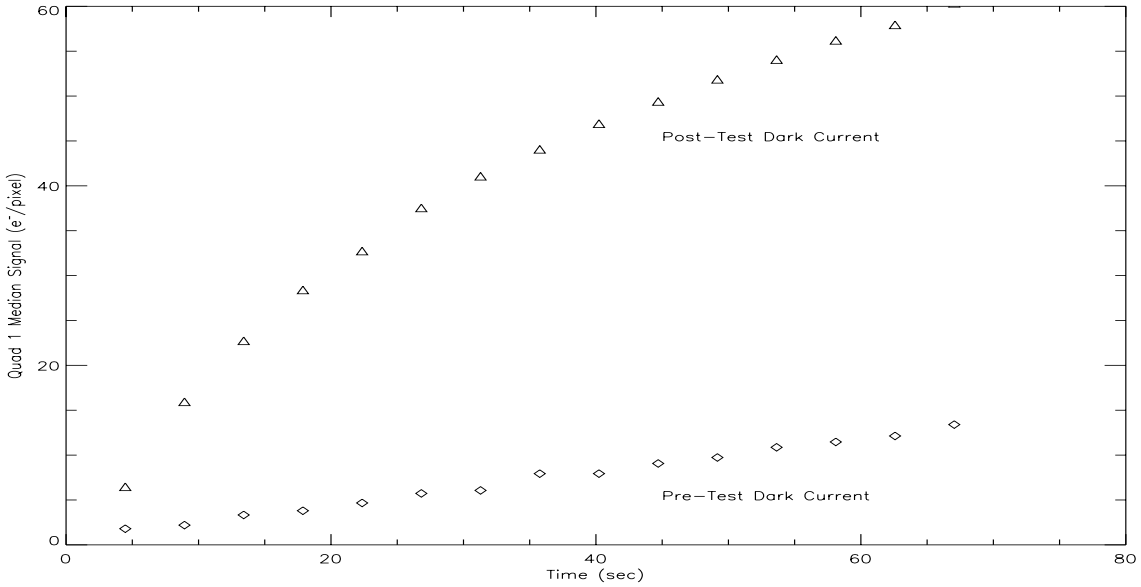

Figure 25: Median signal in quadrant 1 for the pre- and post-illumination dark current ramps. The post-illumination ramp clearly shows the effects of persistence.

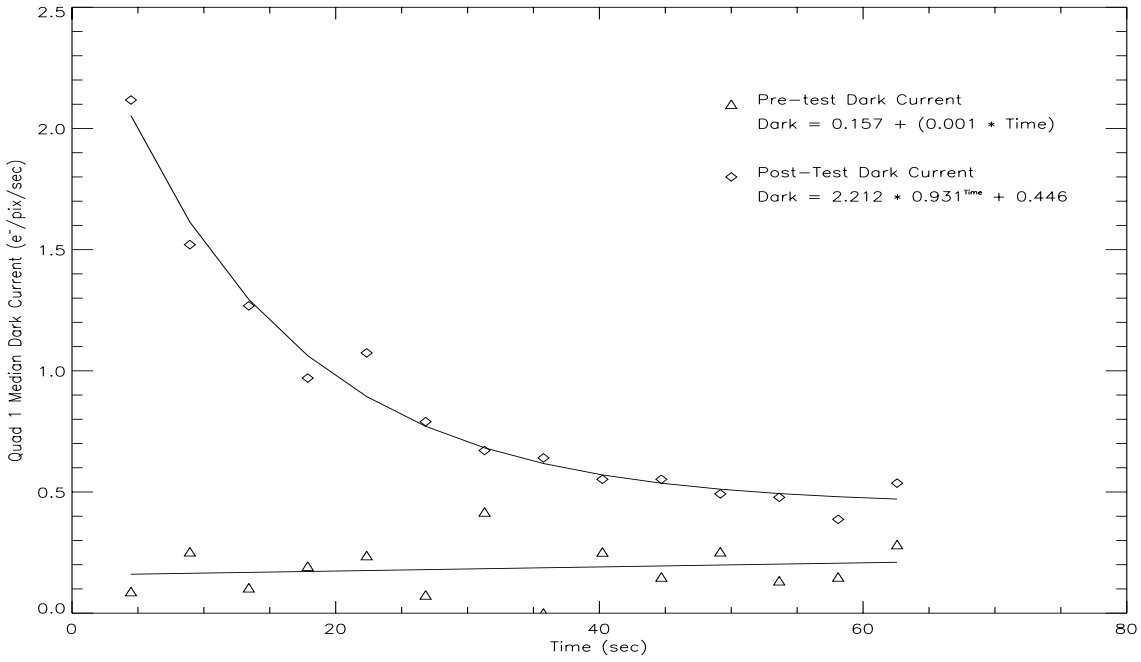

Figure 26: Median dark current in quadrant 1 for the pre- and post-illumination dark current ramps.

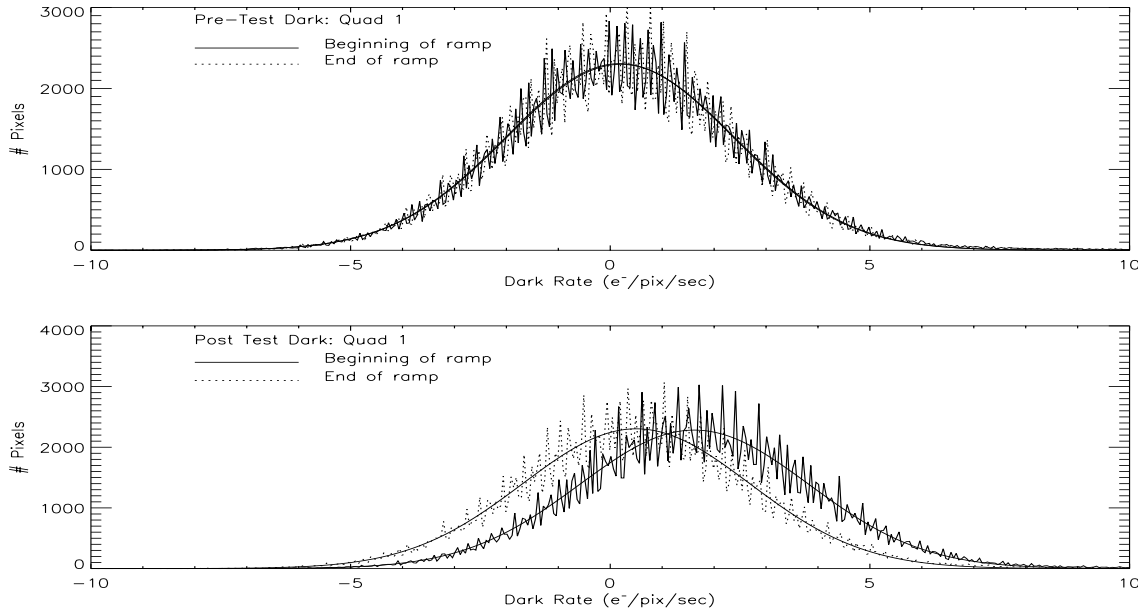

Figure 27: Histograms and gaussian fits to dark currents in quadrant 1 for the pre-illumination (upper plot), and post-illumination (lower plot) dark current ramps. For each ramp, one histogram was made of the dark current map between reads 1 and 2, and a second histogram was made of the dark current map between reads 12 and 13. The dark current decay in the post-illumination ramp leaves the overall shape of the distribution intact.

	Pre-illumination Reads 1-2	**Pre-illumination Reads 12-13**	**Post-illumination Reads 1-2**	**Post-illumination Reads 12-13**
Median Dark Current (e^-/sec/pix)	0.201	0.179	1.619	0.500
Stdev	2.19	2.19	2.21	2.19

Table 11. Characteristics of the Gaussian fits to the histograms shown in Figure 27.

For both ramps, dark current maps at the beginning and end of the ramps were created. Histograms of these dark current maps provided insight into the group behavior of FPA64's pixels. The pre-illumination dark current histograms confirm a nearly constant dark current distribution up the ramp. Gaussian fits to the post-illumination histograms, also shown in Figure 27, reveal a median dark current in quadrant 1 which decreases by ~11% over the course of the ramp. The standard deviation of the distribution is steady at

2.19 e^-/sec/pix across the ramp. These histograms confirm the decrease in dark rate described previously, and show a standard deviation matching that of the pre-illumination dark ramp. It appears that the pixels in FPA64 act largely as a coherent group in their dark current decay rates.

4. Conclusions

Sample Sequence Dark Rates

The median dark current of the WFC3 IR channel, as seen in Table 12, is consistently between 0.10 and 0.21 e^-/sec/pix, regardless of sample sequence, except for observations with the smallest array size and shortest exposure time.

The dark current does not vary with the sample sequence. Figures 7 and 13 show histograms of the median dark current maps for sample sequences with similar exposure times and therefore, signal levels. Figure 28 shows the dark current histograms for SPARS50, STEP50, and MIF600. The total exposure time of these three sample sequences varies by 40%. The histograms for these sample sequences are very similar, with the slightly longer SPARS50 and MIF600 exposures producing histograms with slightly higher and more narrow peaks. Figure 29, which includes data from SPARS100, STEP200, and MIF1500, shows three nearly identical histograms. The exposure times of these three sample sequences vary by only 14%.

Dark Current Variability

The dominant factor in the scatter of dark current values within a given set of identical dark current files is a periodic variation in the dark current tied to variations in the FPA temperature and 6 StageTEC voltage. These variations can cause the dark current to vary by +/- 60-70% around a mean value, given a temperature variation of only 0.3^{o}C.

It also appears that we may have a longer-term, day-to-day variation in the dark current. A comparison of the SPARS10 dark currents from IR01S03, IR01S07, and the manual darks reveals median dark currents of 0.166 e^-/sec/pix, 0.144 e^-/sec/pix, and 0.146 e^-/sec/pix, respectively. None of the individual files in the IR01S03 test had a median dark current as low as the group median values from IR01S07 or the manual darks. All SPARS10 observations were made on the same day, except for the higher dark current files in IR01S03, which were taken 4 days earlier.

The same pattern appears when comparing the RAPID ramps from IR01S03 and IR01S07. The IR01S03 median RAPID dark current was measured to be 0.200 e^-/sec/pix, while those from IR01S07 revealed a median dark current of 0.177 e^-/sec/pix, roughly the same difference seen in the SPARS10 ramps.

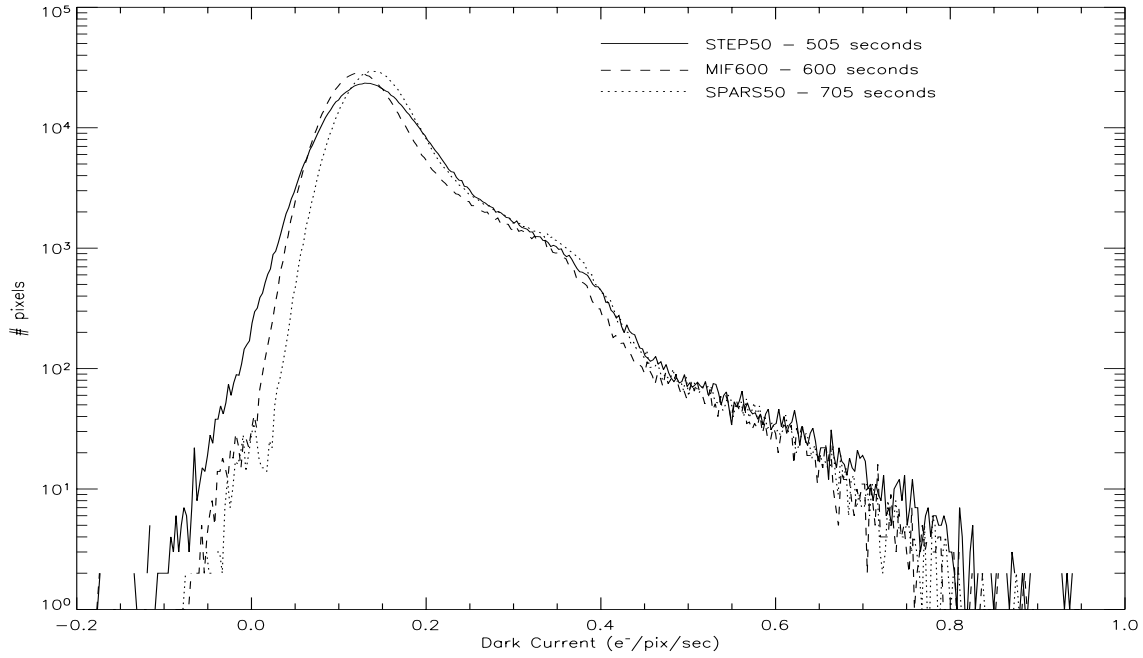

Figure 28: Dark current histograms for the three sample sequences with similar exposure times. STEP50, MIF600, and STEP50 all produce similar dark current histograms, while exposure times vary by 40%.

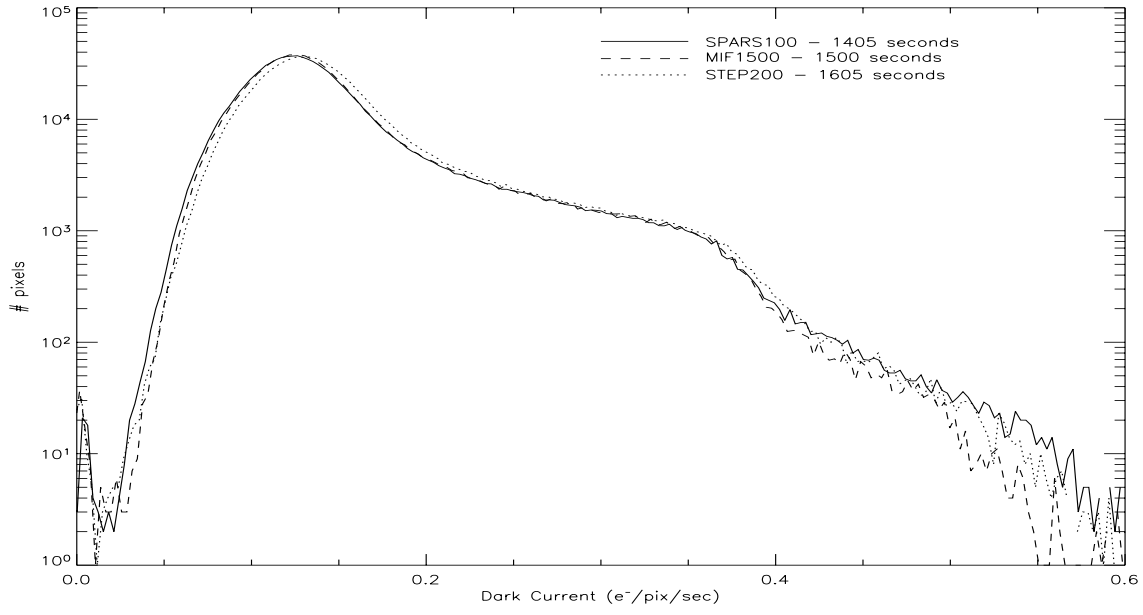

Figure 29: Dark current histograms for three sample sequences with long exposure times. The three sample sequences show very similar dark current behavior. This is expected as total exposure times vary by only 14%.

Masking

From the creation of mask files, it appears that there is a population of hot pixels that changes on a timescale of days. Masks created from data taken 10 days apart show roughly the same number of masked pixels, but with a significant number (~14% of the masked pixels/1.2% of FPA64's total number of pixels) changing positions between the two masks. Over the course of 16 days, 90.9% of the total pixels (935,000) were good in all masks. This rapidly changing population of masked pixels implies that calibration files for FPA64 will have to be taken often, in order to keep the mask current.

Reference Pixels

The inboard reference pixels appear to track changes in the FPA temperature. However, the variation in the reference pixel signal with changing temperature is not enough to compensate for the change in dark current measured in the science pixels.

Spatial Uniformity

The absolute dark current levels of FPA64 vary across the detector. Using the median dark image from all STEP400 files, the dark current variation across the detector was studied. The dark image was divided into 5 x 5 pixel boxes, and the median dark current in each box was calculated. The variations of the 5 x 5 pixel boxes, after smoothing, are shown in Figure 30. Dark rates vary across the detector by 40% from the median in some areas.

The cyclic variation of dark current values with FPA temperature and TEC current is uniform across the detector. No areas on the FPA have been observed with elevated densities of cyclically varying pixels. This suggests that if a temperature variation is the cause behind the variable dark current, the temperature is varying uniformly across the entire detector, rather than being concentrated in one area (e.g near the connection to the TEC).

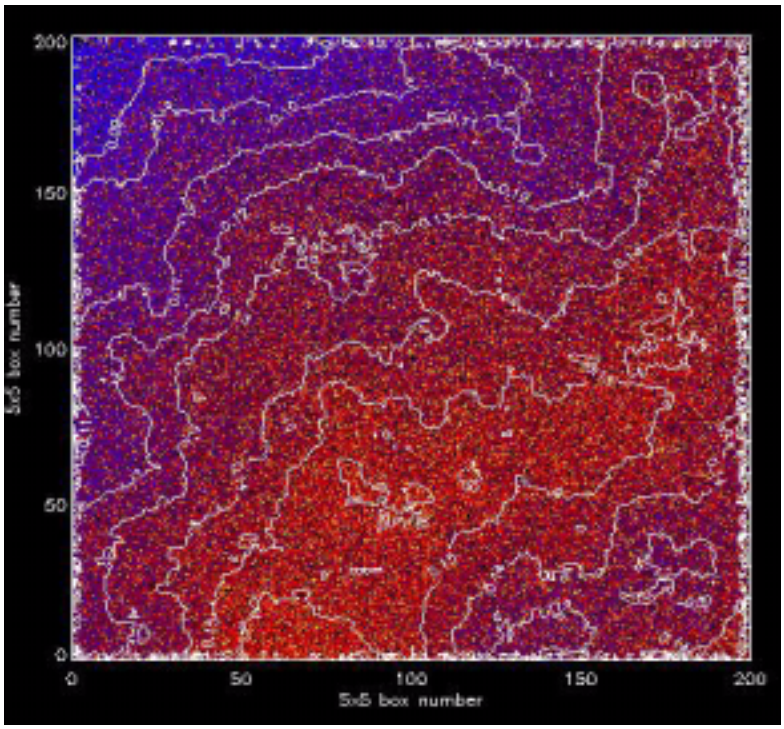

Figure 30: Variation of the dark rate. Values are in units of e^-/sec/pixel. The dark rate in the upper left corner of the detector are 0.09 e^-/sec/pix, while those in the bottom center rise as high as 0.15 e^-/sec/pix.

Persistence

Persistence effects are clearly visible in dark current ramps taken after illumination. The extra signal from the persistence has been observed in dark current ramps taken immediately following, as well as hours after illumination. For files obtained shortly after illumination, the decay of the persistence signal is readily observable. These qualitative conclusions are based on only a few ramps. More data are needed to further investigate and characterize the persistence.

Median Dark Current Values

Table 12 shows the median dark current levels for FPA64 from superdark files created with all of the thermal vacuum test data described in this ISR.

Sample Sequence	Detector Median / Standard Deviation of Dark Current (e^-/sec/pix)	# of Data Files Used
RAPID	0.188 / 0.188	36
SPARS10	0.150 / 0.092	34
SPARS25	0.143 / 0.086	10
SPARS50	0.151 / 0.066	3
SPARS100	0.137 / 0.064	7
SPARS200	0.135 / 0.054	3
STEP25	0.125 / 0.086	13
STEP50	0.145 / 0.072	3
STEP100	0.126 / 0.064	13
STEP200	0.139 / 0.058	3
STEP400	0.135 / 0.058	15
MIF600	0.137 / 0.066	3
MIF900	0.132 / 0.062	3
MIF1200	0.136 / 0.060	3
MIF1500	0.135 / 0.058	3

Table 12. Median full frame and quadrant-by-quadrant dark current for superdark files, created for each sample sequence from all available dark current data from SMSs IR01S02 through IR01S07 and the manual dark current data.

Recommendations

Further investigation into the variation of dark current/temperature/TEC voltage is necessary, in order to understand the cause of the cyclical variations. More data at temperatures significantly different than nominal (IR01S02 had only 2 frames at -127^{o}C), would help to characterize the median dark rate versus temperature relationship.

The large variation in dark current level (~60% - 70%) observed over a small (0.3^{o}C) change in FPA temperature, suggests that FPA temperature should be controlled to much better than the 0.2^{o}C of the current design.

Acknowledgements

Many thanks to Howard Bushouse, and the rest of the WFC3 team for helpful discussions and recommendations regarding dark current analyses for this project.

References

Baggett, W., **Operations and Data Management Plan for the Wide Field Camera 3 (WFC3)**. CDRL no. OP-01. http://www.stsci.edu/instruments/wfc3/WOWG/wfc3-op01-draft.pdf, 2003.

DCL, **Detector Test Results, Rockwell HgCdTe for HST WFC3 Project**, http://dcl.gsfc.nasa.gov/private/wfc3/webwebdocs/fpa64/FPA64.html, April 2003.

Hilbert, B., **Basic IDL Data Reduction Algorithm for WFC3 IR and UVIS Channel**. ISR WFC3-2004-10. http://www.stsci.edu/hst/wfc3/documents/ISRs/WFC3-2004-10.pdf. June 2004.

Hilbert, B., Baggett, S., and Robberto, M., **Masking Technique on WFC3-IR Images**. ISR WFC3-2003-06. http://www.stsci.edu/hst/wfc3/documents/ISRs/WFC3-2003-06.pdf. May 2003.

Robberto, M., Hanley, C., and Dashevsky, I., **The Reference Pixels on the WFC3-IR Detectors**. ISR WFC3-2002-06. http://www.stsci.edu/hst/wfc3/documents/ISRs/WFC3-2002-06.pdf. June 2002.